Talanta 204 (2019) 713–730

Contents lists available at ScienceDirect

Talanta

journal homepage: www.elsevier.com/locate/talanta

Ammonia gas sensors: A comprehensive review

Dongwook Kwak[a,b,*], Yu Lei[c], Radenka Maric[b,c,d]

[a] Institute of Materials Science, 97 North Eagleville Road, University of Connecticut, Storrs, CT, 06269, USA
[b] Center for Clean Energy Engineering, 44 Weaver Road, CT, 06269, USA
[c] Department of Chemical and Biomolecular Engineering, University of Connecticut, 191 Auditorium Road, Storrs, CT, 06269, USA
[d] Department of Materials Science and Engineering, 97 North Eagleville Road, University of Connecticut, Storrs, CT, 06269, USA

ARTICLE INFO

Keywords:
Ammonia
Gas sensor
Metal oxide
Conducting polymer
TDLAS
Electrochemical
Surface acoustic wave
Field effect transistor

ABSTRACT

In recent years, sensitive, selective and accurate sensing techniques for ammonia gas detection have been highly demanded since ammonia is both a commonly utilized gas in various industrial sectors and a highly toxic and corrosive agent that can threat human health and environment. This review article discusses the widely used gas sensing techniques in ammonia detection. The fundamental working principles of the ammonia detection techniques relying on electronics, electrochemistry, tunable diode laser spectroscopy, surface acoustic wave, and field effect transistors are briefly described first, in conjunction with various sensing materials. Furthermore, recent progress in the development of advanced ammonia gas sensors was comprehensively reviewed and summarized. Finally, the outlook for future development of high-performance ammonia sensors was presented.

1. Introduction

In the last decades, novel gas sensors have been developed and employed in diverse fields for applications such as environmental analysis, automotive industry, medical applications, and indoor air quality controls [1–4]. Especially, there has been an increasing need for monitoring hazardous gases including CO, CO_2, NO_x (x = 0.5, 1, and 2), SO_x (x = 2 and 3), and NH_3 as concerns over environment and human health grow. Among these perilous gas species, ammonia (NH_3) gas detection has attracted substantial attention in the field of gas sensor, which is important because NH_3 is one of the most common chemicals manufactured and applied in diverse areas around the world [5–11]. Recently, around 80% of NH_3 has been produced for the nitrogen-based fertilizer and the rest of 20% has been manufactured for pharmaceuticals, cleaning products, explosives, and refrigeration by following the Haber-Bosch process (Eq. (1)) which employs the reaction between hydrogen and nitrogen with an iron-based catalyst under high temperatures (~500°C) and high pressures (~300 bar) [12].

$$3H_2 + N_2 \rightarrow 2NH_3 \quad \Delta H_{300} = -46.35 KJ/mol,\ \Delta S_{300} = -99.35\ J/Kmol \tag{1}$$

In our daily life, the usage of NH_3 is easily found in dairy and ice cream plants, wineries and breweries, petrochemical facilities, fruit juice, and vegetable juice and soft drink processing facilities [12,13]. Additionally, since NH_3 is a great source of hydrogen, it is often utilized in automobiles, specifically diesel engines, to reduce harmful NO_x gases by selective catalytic reduction (SCR) as shown in the following reducing reaction [9,10,14]:

$$4NO + 4NH_3 + O_2 \rightarrow 4N_2 + 6H_2O \tag{2}$$

Lately, about 2.1–8.1 Tg of NH_3 has been emitted into the atmosphere every year through human activities [13]. In the atmosphere, the typical NH_3 level is in low ppb (1–5 ppb) levels [15]; however, inhaling more than the safe level of NH_3 can trigger life-threatening illnesses due to its highly toxic and corrosive properties to the skin, eyes, and lungs. According to Occupational Safety and Health Administration (OSHA), the exposure limit of NH_3 to human beings is 25 ppm for 8 hours and 35 ppm for 10 minutes [14,16]. Additionally, NH_3 is considered an environmental pollutant since it is highly reactive and forms aerosols such as ammonium nitrate and ammonium sulphate when it reacts with nitric acid and sulfuric acid in the air, respectively. As a result, these nanosized NH_3 aerosols create smog that exhibit a temperature reducing effect and, consequently, a negative impact on the global greenhouse balance [13,17,18]. Moreover, since exhaled NH_3 in the human breath is one of the critical biomarkers to diagnose lung or renal diseases, monitoring NH_3 by means of breath analyzers is a very important daily routine of clinical practice for people who suffer from those diseases. Therefore, the accurate measurement of NH_3 gas has been in demand to prevent fatal accidents caused by overexposure to NH_3 as well as the environmental problem occurred by increased

* Corresponding author. Institute of Materials Science, 97 North Eagleville Road, University of Connecticut, Storrs, CT, 06269, USA.
E-mail address: dongwook.kwak@uconn.edu (D. Kwak).

https://doi.org/10.1016/j.talanta.2019.06.034
Received 12 March 2019; Received in revised form 8 June 2019; Accepted 8 June 2019
Available online 15 June 2019
0039-9140/

emissions of NH_3 to the atmosphere, and lethal diseases indicated by high concentrations of exhaled NH_3 in human breath [19–21].

Recently, extensive interest in improving reliable NH_3 gas sensors has been rising as innumerable fields employing NH_3 gas sensors has been expanding. Similar to other gas sensors, advanced NH_3 gas sensors must exhibit major aspects including sensitivity, selectivity, stability, and reversibility, and, trivially, broad range of measurement and operation temperatures, safety, low price, compactness, light weight, etc. as minor properties. For a brief description of the major important aspects: (1) sensitivity refers to the ability of sensor to detect the minimum concentration of target gas; (2) selectivity is the capability of sensor to distinguish a particular gas among a gas mixture; (3) stability represents how stable the sensor is during the operation under severe conditions as high temperature, high pressure, and corrosive environment; (4) reversibility is the ability of sensing material that is able to restore its initial state after reaction with a target gas [12,13]. To satisfy these critical aspects and enhance the sensing performance, miscellaneous detection techniques for NH_3 gas sensing have been explored and studied [13,22]. This review begins with the sensing mechanism and working principles of the most prevalent NH_3 gas sensing methods as classified in Fig. 1. Moreover, the recent progress of the ammonia gas detection techniques is discussed and, finally, this review will be concluded with a discussion of future trends in the development of advanced NH_3 gas detection.

2. Ammonia gas sensing methods

There are a variety of sensing techniques existing for NH_3 detection; however, the most prevalent detecting methods can be classified into three major categories, which are the solid-state sensing methods (metal oxide-based sensors, and conducting polymer sensors), the optical method (optical sensors utilizing tunable diode laser spectroscopy), and other methods (electrochemical sensors, surface acoustic wave sensors, and field effect transistor sensors). Based upon the sensing materials and detecting techniques, not only their sensing mechanisms and working principles as NH_3 gas sensors, but their recent progress will be also discussed in the following chapters.

3. Solid-state sensing methods

3.1. Metal oxide-based sensors

Due to its advantages such as simplicity, low cost and flexibility in fabrication, and good process compatibility, metal oxide-based gas sensors have attracted significant attention in the gas sensing field and, especially, SnO_2, ZnO, WO_3, TiO_2, and MoO_3 are the most widely utilized metal oxides in NH_3 detection [23–26]. Basically, as a gas sensing material, metal oxides are classified into n-type and p-type semiconducting metal oxides and represent its promising electrical properties in the temperature range between 250 °C and 550 °C. Mostly, the n-type semiconducting metal oxides are selected for gas detection due to the inferior gas sensing response of the p-type semiconducting metal oxides and the response relationship between those two types of metal oxides is as follows [27],

$$S_p = \sqrt{S_n} \tag{3}$$

where S_p and S_n denote the gas sensor response of p-type and n-type semiconducting metal oxides, respectively.

In general, the electronic structure of the metal oxide is a key factor in terms of selecting an appropriate metal oxide for detecting specific gases [28] and also an important characteristic to understand the sensing mechanism. Furthermore, it can be used to categorize metal oxides into the transition and the non-transition-metal oxides [29], for example:

(1) Non-transition-metal oxides, which contains (a) pre-transition-metal oxides (MgO, Al_2O_3, etc.) and (b) post-transition-metal oxides (ZnO, SnO_2, etc.).
(2) Transition-metal oxides (Fe_2O_3, NiO, Cr_2O_3, etc.)

The non-transition-metal oxides have only one oxidation state and it exhibits an inferior electrical characteristic as a sensing material, compared to the transition metal oxides which have more than one oxidation state [30–32]; however, not all of the transition metal oxides are selected as a sensing material since only transition-metal oxides with d^0 and d^{10} electronic configurations can be used for gas detection [33]. Although the post transition metal oxides belong to the non-transition group, some of them which have the d^{10} electronic configuration are frequently utilized for gas detecting applications. This might be attributed to the fact that the post-transition-metal oxides retain cations with the filled d^{10} orbital configuration and are reduced to generate free electrons when it is reacted with reducing agents, such as NH_3 [31–33].

In addition to the electronic structure model, the energy band model, also known as the double-Schottky barrier model is often employed to understand the sensing mechanism of metal oxide based NH_3 sensors. Under an oxygen atmospheric condition, the potential barrier at the grain boundaries increases since the charged atmospheric oxygen molecules form a depletion layer by trapping electrons from the surface of metal oxides and, as a result, the overall conductivity decreases. On the other hand, when the reducing gas is introduced, the reverse phenomenon occurs and, consequently, the height of the barrier is lowered, resulting in an increase of the conductivity [13,28,34–37]; however, this can be only observed in n-type semiconducting metal oxides with relatively smaller depletion areas than its grain size.

Although the metal oxides have attractive advantages as a gas sensing material, serious shortcomings should be addressed, such as low selectivity in detecting one particular gas from gas mixture [13,28,38].

In the field of metal oxide-based gas sensors, there have been immeasurable efforts to enhance its sensitivity and selectivity and lower its operation temperature since its first appearance in the 1950s [39]. Since the local shifting of electronic charge at the surface of metal oxides plays an important role in detecting gases, adding second phase materials onto the oxide surface is one of the widely utilized methods to improve the sensing performance of metal oxide-based gas sensors [40]. This method is based upon the charge carrier diffusion process that

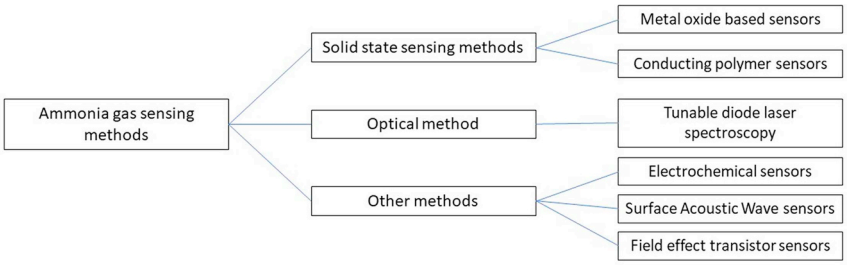

Fig. 1. Categorization of ammonia gas sensing techniques.

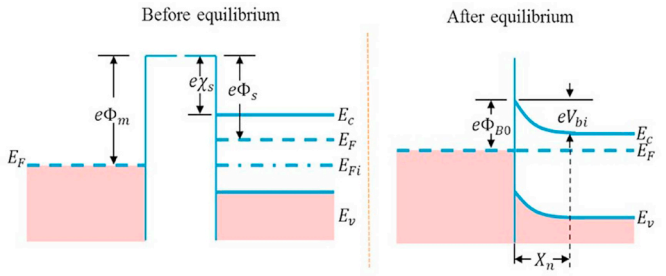

Fig. 2. Schematic diagram of the Schottky junction [41]. Reprinted with permission from ref. 41.

electrons at a higher Fermi energy state shift across the interface until the Fermi energy across the junction is leveled when the intimate electrical contact is created at the interface between two different materials. With the use of this phenomenon, the surface conductivity of metal oxides can be regulated for enhanced gas detection. The presence of a noble metal with a high work function on the surface of an n-type metal oxide semiconductor, for example, facilitates electrons to flow from the semiconductor to metal until an equilibrium state at the Fermi level is achieved, creating a Schottky barrier shown in Fig. 2 [41].

As a result, a wide depletion region in the semiconductor is formed, resulting in a significant decrease in conductivity [42]. The wide depletion area in the semiconductor causes a large Fermi level-difference that facilitates the gas sensing performance [42]. The width (W) of the space charge region is defined by [40],

$$W = \left[2\varepsilon V_{bi} / eN_D \right]^{1/2} \quad (4)$$

where ε is the static dielectric constant, V_{bi} is the built-in voltage, e is the electrical charge, and N_D is the donor concentration. Furthermore, the catalytic characteristic of the noble metal aids by either lowering the operation temperature or increasing the tolerance against relative humidity [43]. The noble metals such as platinum, palladium, gold, silver, etc., are typically employed to enhance the performance of metal oxide gas sensors and their work functions are given in Table 1 [40].

Zeng et al. [44] demonstrated the Pd-doped ZnO based NH_3 sensor that yields an enhanced sensing performance towards NH_3. In addition to the interpretation of the improved sensing property by the schottky junction, the enhancement of their system in response and recovery times and the operation temperature also can be explained by the formation of a weak-bonded complex between Pd atoms and the oxygen gas at relatively low temperature [45]. When the Pd-doped ZnO surface is exposed to NH_3, the weak-bonded complex of Pd and oxygen is quickly dissociated to produce oxygen atoms that move along the surface of grains and start trapping electrons from it to yield additional chemisorbed oxygen atoms (O_2^-, O^{2-}, O^-). The reaction between NH_3 and the adsorbed additional oxygen atoms is then activated by the catalyst (Pd) atoms and, as a result, more electrons generated from the reaction are released back to the conduction band of ZnO. This leads to the enhanced sensitivity at relatively low operation temperature. With their Pd-sensitized ZnO nanostructure based NH_3 sensor, the detection limit of 5 ppm of NH_3 was achieved and 3 seconds(s) and 9 s were

Table 1
Work function ranges of the noble metals used to enhance the gas sensing properties of metal oxides. Regenerated from ref. [40].

Metal	Work function (eV)
Platinum	5.22-5.6
Palladium	5.12-5.93
Gold	5.1-5.47
Silver	4.26-4.74

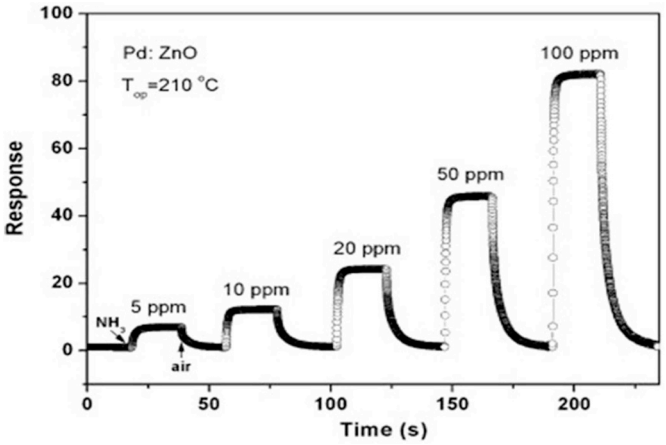

Fig. 3. Responses of the pure and Pd-doped ZnO nanostructures to NH_3 at different concentrations [44]. Reprinted with permission from ref. 44.

obtained for the response and recovery times, respectively as shown in Fig. 3.

A further enhanced structure in the decoration of metal oxides with secondary phase materials is the ternary nanocomposite normally consisting of noble metals, metal oxides, and graphene and has been reported by Su et al. [46]. They suggested a Pd/SnO_2/RGO (reduced graphene oxide) ternary nanocomposite based NH_3 gas sensor that shows the enhanced sensing performance at room-temperature. Not only did the catalytic activity of Pd improve the sensor response, but RGO was also critically involved in the enhancement of gas sensing property in their system. The RGO doping into the Pd/SnO_2 film reduced the film resistance to ~100 kΩ, while a high resistance was observed from the pure SnO_2 film in comparison. The decrease in resistance is attributed to the fact that the RGO is conductive and produces new electrical routes in the Pd/SnO_2/RGO ternary nanocomposite film and, consequently, the overall sensor response is improved by facilitating the charge transfer in the film. According to their report, the response of the Pd/SnO_2/RGO film to 5 ppm of NH_3 gas was 7.6, whereas that of the Pd/SnO_2 film to 100 ppm of NH_3 gas was 8, which is defined by a following equation [46],

$$S(response, \%) = R_{air} - R_{Gas} / R_{air} \times 100\% \quad (5)$$

The performance enhancement of metal oxide-based NH_3 gas sensor can also be achieved by adding a metal oxide dopant into another metal oxide base. For example, Qi et al. [47] suggested the SnO_2 nanoparticle-coated In_2O_3 nanofiber structure for improved NH_3 detection at room temperature. Since both In_2O_3 and SnO_2 have excellent chemical stability, versatility, and controllability, as gas sensing materials, hybridization of the two metal oxides creates a great synergy in that the SnO_2 nanoparticles on the In_2O_3 nanofibers provide the more reacting sites for gas molecules [48–50]. As shown in Fig. 4, the sensor performance of the SnO_2 nanoparticle-coated In_2O_3 nanofibers is better than that of pure In_2O_3 nanofibers when it comes to the sensor response, response time, and recovery time. In comparison of those two structures, the sensor response is improved from 4 to 21, while the response time decreases from 16 to 7 s, and the recovery time also decreases from 15 to 10 s at 1 ppm NH_3.

Wang et al. [51] demonstrated an enhanced NH_3 gas sensor using the Co_3O_4/SnO_2 hybrid core-shell nanosphere (HCSNS) constructed in a unique structure as shown in Fig. 5. The enhanced sensing property is attributed to its structural advantage that provides additional reaction sites for analyte gas molecules and increases the effective absorption speed. Additionally, the formation of an additional depletion layer and potential barrier in the Co_3O_4/SnO_2 heterojunctions contributes to improving the sensor performance. The additional depletion layer and

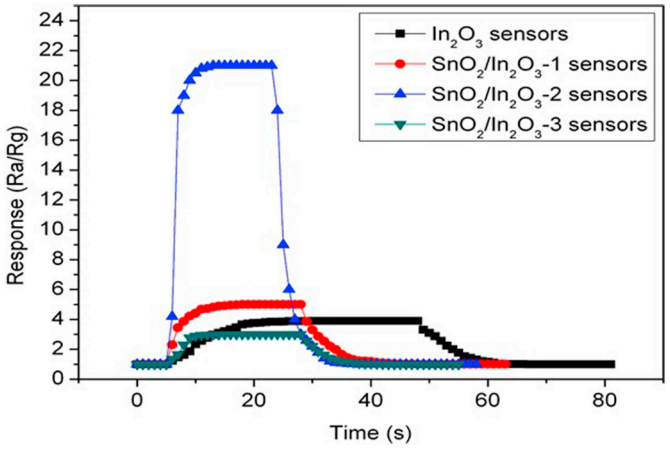

Fig. 4. Response-time curves to 1 ppm NH_3 at RT of In_2O_3 and SnO_2/In_2O_3 sensors [47]. Reprinted with permission from ref. 47.

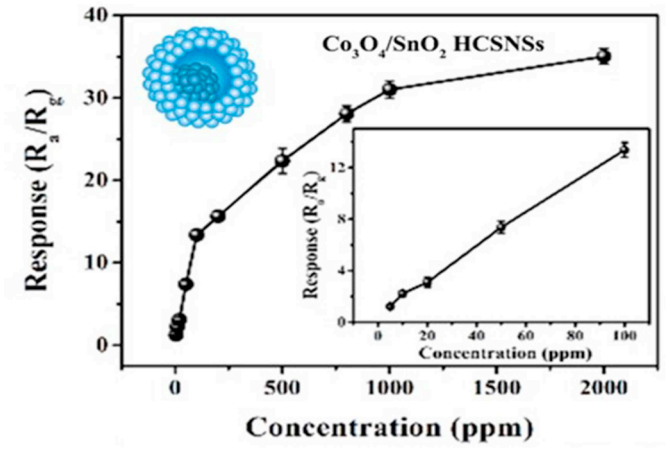

Fig. 5. Sensor response in various concentrations of NH_3 at 200°C. Inset: enlarged response curve from 5 to 100 ppm of NH_3 [51]. Reprinted with permission from ref. 51.

potential barrier were formed by the p-type Co_3O_4 trapping electrons generated from SnO_2 and, consequently, the resistance of Co_3O_4/SnO_2 significantly increased. On the other hand, when the sensing film was exposed to NH_3 gas, the trapped electrons released back into the conduction bands of Co_3O_4/SnO_2 and the total resistance of the sensor dramatically decreased. As a result, an improved sensing performance was obtained as fast response time of 4 s, recovery time of 17 s, high response of 13.6 and good selectivity at 200°C.

3.2. Conducting polymer sensors

Since the advent of conducting polymers, a great number of gas sensors have utilized conducting polymers due to its advantages, such as, ease in fabrication and modification, stability, design flexibility, tunability with other materials, etc. [52–58] Amongst the conducting polymers, polypyrrole, polyaniline, and polythiophene are by far the most frequently used in the gas sensor field [13,59,60] and the active layers in gas sensors consist of these conducting polymers. Although conductometric, potentiometric, amperometric, colorimetric, and gravimetric modes are mostly employed as operation method for conducting polymer-based sensors [61,62], a great number of gas sensors using conducting polymer are based on the amperometric mode utilizing the redox reaction between a target gas and the conducting polymer to detect a particular gas [63]. For instance, when PPy interacts with NH_3 gas, the doublet of nitrogen in the polymer backbone loses its electron and this electron transfer between the positive holes of PPy and NH_3 molecule causes a decrease in the charge-carrier concentration, which lowers the overall conductivity [64]. The interaction mechanism between PPy and NH_3 is as following,

$$PPyH^+ + NH_3 \rightarrow PPy + NH_4^+ \quad (6)$$

In the air, the reverse reaction that NH_4^+ ion decomposes into ammonia takes place and changes the conductivity of PPy to an increase.

There are various configurations using conducting polymers as the NH_3 gas sensing active layer: transistor and diode sensors, optic sensors, piezoelectric crystal sensors, amperometric sensors, and chemiresistors. The most common configuration of conducting polymer NH_3 gas sensors is the chemiresistor and its detection limit is relatively low (< 10 ppm) compared to other configurations in this category [63,65]. The quick response time is also a huge advantage of the chemiresistor, which is about hundreds of seconds and, even few seconds obtained from super-thin film gas sensors [65–67].

There has been so much attempt in enhancing the sensor performance of conducting polymer-based gas sensors by improving physical and electrical properties of conducting polymers by means of the modification of its structures and the use of dopants added into it [68]. Modifying the structure of conducting polymer plays a very important role in developing conducting polymer based NH_3 gas sensor in that the developed structure significantly improves the sensing film properties such as facilitating electron or proton transfer and ensuring the better interaction between the sensing film and analyte gases. Especially, nanostructures have attracted great attention in modification of conducting polymer due to its high surface-to-volume ratio and small dimensions, which leads to the improved interaction between the materials and analytes and the fast adsorption/desorption kinetics for analytes, resulting in high sensitivity, and quick response and recovery times, respectively [68]. In addition to the enhanced sensing performance, the nanostructured conducting polymers have also satisfied the miniaturization in sensor packaging. For instance, polyaniline (PANI) nanofiber shows enhanced sensing performance due to its large specific surface area and interconnected network structure. The sensing mechanism of PANI nanofiber to NH_3 is the same as the eq. (6). In the presence of NH_3 gas, the sensing film is deprotonated and the deprotonation rate relies on the concentration of NH_3, resulting in an increase of the film resistance. In contrast, as the sensing film is exposed to the air, the ammonium ions decompose into ammonia molecules and protons which restore the original doping level of PANI. Consequently, this decomposition leads to a decrease of the film resistance [69]. Du et al. [70] reported that the NH_3 gas sensor based on the 4-toluenesulfonic acid (TSA) doped PANI nanofibers on interdigitated array electrodes represents rapid response time (10 s) and quick recovery time (100 s) at 50 ppm NH_3 gas. According to their report, the PANI nanofiber film also shows a better sensitivity (1.06), compared to a convention PANI film (0.3) for 50 ppm NH_3 gas. The improved sensor response and sensitivity could be attributed to the fact that more NH_3 molecules are able to diffuse into their nanofiber film and react with active site of PANI chains swiftly because of its large specific area resulting from the small diameter and the interconnected network of PANI nanofibers (see Fig. 6).

Although the structure modification of conducting polymer is able to impressively improve the sensing performance, the method itself has limitation due to the intrinsic shortcomings of conducting polymer, such as poor mechanical strength, sluggish reaction kinetics, and specificity. For addressing these shortcomings, adding either organic or inorganic materials as a dopant into the conducting polymers has been widely utilized [41]. Wojkiewicz et al. [71] achieved the ppb level of NH_3 detection with two different PANI-based systems consisting of the polyvinylidene fluoride (PVDF) and polybutyl acrylate (PBuA) core-shell particle-based structure, and an amorphous dielectric polyurethane (PU) matrix based PANI nanofiber structure. To generate a

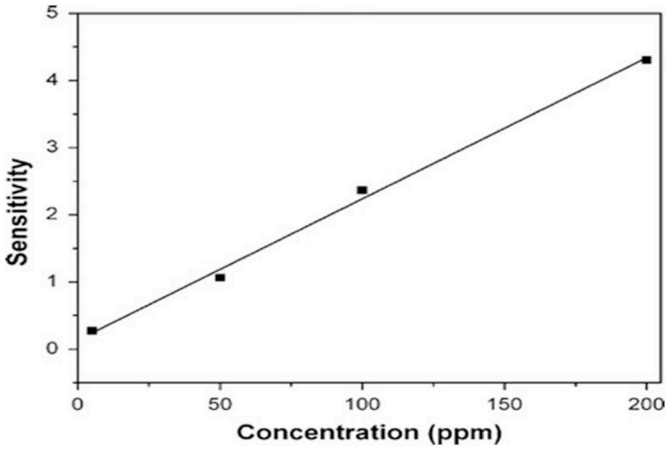

Fig. 6. Sensitivity of PANI nanofiber sensor on different NH_3 concentrations [70]. Reprinted with permission from ref. 70.

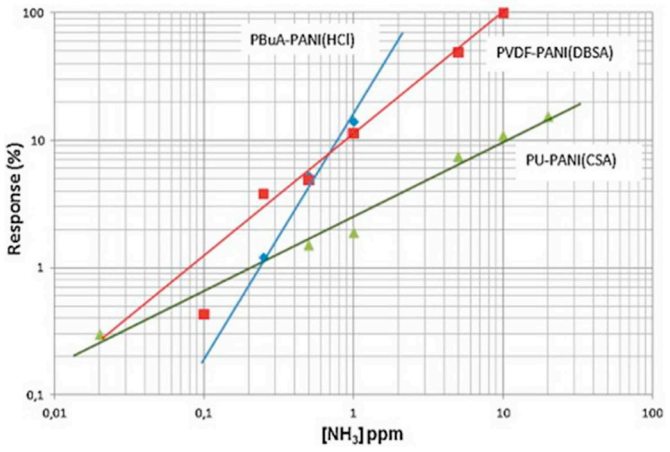

Fig. 7. Response of the core-shell based sensors (PDVF-PANI(DBSA) and PBuA-PANI(HCl)) and PU matrix-based sensor [71]. Reprinted with permission from ref. 71.

response plot of the sensor as a function of NH_3 concentration, they applied a definition from the literature: the quotient of the variation of the response of the sensor is determined by the corresponding variation of the NH_3 gas concentration [72]. As shown in Fig. 7, the lowest detection limit (20 ppb) was achieved by the PU-PANI$(CSA)_{0.25}$ nanocomposite, while the higher sensitivity (the slope) was obtained from the core-shell based nanocomposites. The different trend between the sensitivity and the detection limit might be attributed to the fact that the higher film conductivity resulting from the more uniform and smoother surface of PU-PANI$(CSA)_{0.25}$ leads to a more effective charge transport in PANI$(CSA)_{0.25}$ and the lower detection limit in comparison with the core-shell based nanocomposites. On the other hand, since the sensitivity highly depends on the specific surface area where the reaction with the analyte gas occurs, the core-shell based nanocomposites with more porous structures showed a higher sensitivity than the PU-PANI$(CSA)_{0.25}$ nanocomposite in their system.

The typical inorganic materials for supporting conducting polymers in NH_3 sensing are copper, gold, silver, and platinum owing to their catalytic characteristic [73–75]. Especially, the nanoparticle form of these catalysts plays a critical role in improving the sensor performance in that it eases the charge transfer across conjugated chains and the interaction with the analyte gas. Patil et al. [76] utilized Cu nanoparticles as a support material in a thin sensing layer of PANI nanocomposites to enhance the conductivity, thermal stability, and adsorption/desorption of analyte gases on the surface of sensing film. According to their report, the Cu content ratio to PANI is important since the sensing performance increases as the concentration of Cu increases; however, once the concentration of Cu reaches its optimum level (0.13 at%), the sensor performance deteriorates because of its shunting effect between metal and semiconductor. With the optimum concentration of copper, their copper nanoparticle intercalated-PANI nanocomposite film showed the superior sensing performance to that of the pristine PANI film and can detect gaseous NH_3 as low as 1 ppm, and it shows the fast response time (7 s), and recovery time (160 s) at 50 ppm in room temperature (see Fig. 8).

4. Optical method (tunable diode laser absorption spectroscopy, TDLAS)

Gas sensors utilizing optical absorption have attracted immense attention as they are able to overcome obstacles that other gas sensors using contact-sensing techniques generally have, e.g. measurement error from the long-term memory effect [77]. Also, this technique is very appealing in commercialization due to its simplicity to operate and ability to achieve very high selectivity, fast analysis, and great sensitivity along with relatively long-life time [78,79]. Moreover, this method shows attractive properties in gas detection since it can be operated at a wide range of temperatures (from room temperature to temperatures as high as 1500°C), under unstable pressures, and in highly perilous and corrosive environments.

Amongst gas sensors using optical absorption, the tunable diode laser absorption spectroscopy (TDLAS) has been well-developed for NH_3 gas detection [80]. As shown in Fig. 9, many critical gas species including NH_3 show its absorption in the infrared spectral region and the gases whose molecules are rovibrationally excited in the infrared line-spectrum by the laser light can be detected by this technique. Typically, for NH_3 gas detection, the wavelength in the spectrum range from 1450 to 1560 nm (~6400–6900 cm^{-1}) is chosen [81].

The NH_3 concentration measurement of TDLAS is based upon the absorption spectroscopy and employs the Beer-Lambert law which is [82,83],

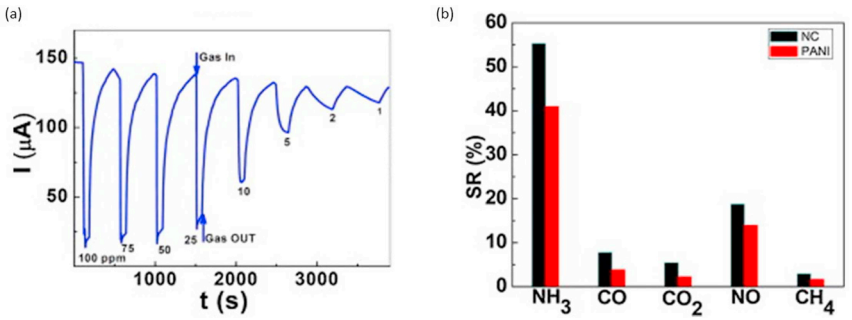

Fig. 8. Response curve to different concentrations of NH_3 at RT (a) and selectivity histogram (b) of the Cu nanoparticle intercalated-PANI nanocomposite film [76]. Reprinted with permission from ref. 76.

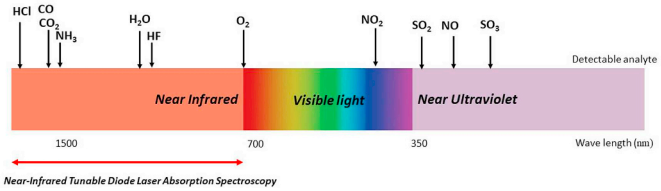

Fig. 9. The detectable analytes in the electromagnetic spectrum.

$$I_v = I_{v0}\cdot\exp\left[-S\cdot\Phi_v\cdot N\cdot l\right] = I_{v0}\cdot\exp\left[-\alpha\right] \quad (7)$$

where I_v is the transmitted laser intensity with the frequency v through an absorbing medium, I_{vo} is the initial laser intensity, S is the temperature dependent line strength of an absorption line, Φ_v is the line-shape function, N is the fractional concentration of the analyte, and l is the path length of the laser through the medium. In addition, on the right formula, α is the absorbance and represents the relationship between the two laser intensities:

$$\alpha(v) = -\ln\left(I_v/I_{v0}\right) \quad (8)$$

A basic configuration of TDLAS for NH_3 gas detection is shown in Fig. 10 and it mainly consists of the laser emitter, the photodetector, the analyte gas chamber, the reference cell, the pressure and temperature control unit, and the electronic analyzer [84–86]. Once the tuned light from the semiconductor laser emitter launches, it is split and passes through the NH_3 gas chamber and the reference cell simultaneously and reaches each photodetector. When the emitted light arrives at the photodetector, it is converted into an electrical signal and used to calculate the analyte concentration.

Since the laser sources and spectroscopic techniques play an important role in TDLAS, there has been incessant attempts to enhance TDLAS with substantial improvements in advanced diode laser sources and laser spectroscopic techniques [87–89]. Although TDLAS has splendid advantages, such as simplicity in operation, high sensitivity and selectivity to a specific analyte gas, noninvasive detection, environmentally friendly analysis (i.e., no harmful chemical usage and hazardous by-products to the environment), etc. [90], the inherent limitation of the laser source in TDLAS systems hinders its robust measurements in gas detection. For example, although semiconducting laser diodes have attractive aspects, such as the compactness and efficiency in configuration, it requires very high threshold currents and cryogenic temperatures to confine carriers to the junction region due to its intrinsic large losses during operation [90]. In addition, sensitivity to temperature and current variations, limited output power, and acoustic vibrations are also known as serious drawbacks of the use of semiconducting laser diodes. To address such issues, advanced diode laser sources have been introduced [91]. Amongst the developed diode lasers, quantum cascade lasers (QCLs) have been frequently selected as a laser source in the enhanced TDLAS systems due to their capability of high resolution, room-temperature operation, and ultra-sensitive and selective analyte gas monitoring [92–95]. QCLs are distinct from conventional diode lasers in that the laser transition takes place between the quantized states restricted mostly in the conduction band of the semiconductor heterostructures, which means that only one type of carrier, primarily electrons, is involved in the optical process. Due to its distinct optical transition phenomenon, the emission wavelength of QCLs can be tuned by simple adjustments on the thickness of the heterostructure wells and barriers. This is greatly beneficial in reducing the reliance on the bandgap of the heterostructure materials and leads to broad tuning range that is directly related to the performance improvement of the laser source in gas sensing [96–99]. In addition, the single mode emission with a narrow linewidth for high selective gas detection can be also attained in using QCLs [100]. Since narrow linewidth and single longitudinal mode operation of QCLs are critical for accurate spectroscopic measurements in gas detection, a distributed feedback (DFB) structure at a precisely selected wavelength by introducing a periodic grating structure on the top of the QCL waveguide is also widely incorporated with QCLs for improved resolution spectroscopy applications [101–103] (see Fig. 11).

Miller et al. [104] demonstrated a QCL based NH_3 gas sensor and achieved the detection limit is 0.15 ppbv at 10 Hz with the use of the continuous-wave, DFB QCLs and HgCdTe photodetectors. In addition, the precision and stability of their sensor was determined by Allan deviation analyses [105]. Their sensor is advantageous over other typical close-path sensors in that sampling artifacts can be reduced dramatically and any pumping or heating systems are not required. Therefore, improved detection and lowered power consumption can be achieved (see Fig. 12).

Recently, Tao et al. [106] reported a low-power and open-path mobile sensing platform for NH_3 gas detection by integrating multiple open-path QCL based sensors and mobile sensor systems. Specifically, one of the four open-path optical gas sensors in their integrated sensing platform is the NH_3 gas sensor with the light source of 9.06 μm QCL that has the detection limit of 150 pptv at 10 Hz. Lewicki et al. [107] also utilized a DFB QCL to achieve a real time room-temperature (RT) NH_3 detection with the detection limit of 6 ppb with 1 s time resolution.

In general, TDLAS for highly sensitive and selective gas sensing requires a long optical pathlength and, as a result, a sizeable stationary configuration (e.g., long path multipass cells) has been generally accepted [108]; however, it could give rise to an issue with respect to

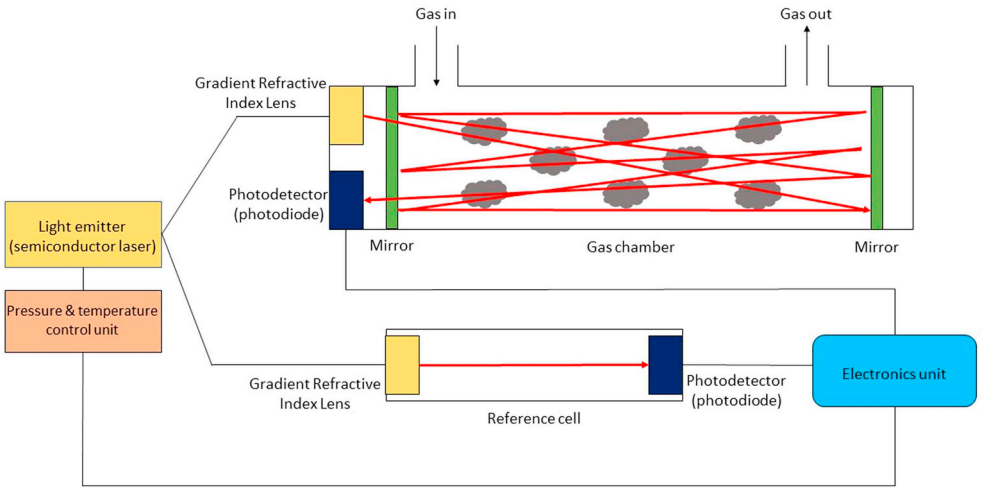

Fig. 10. A schematic configuration of TDLAS for gas detection.

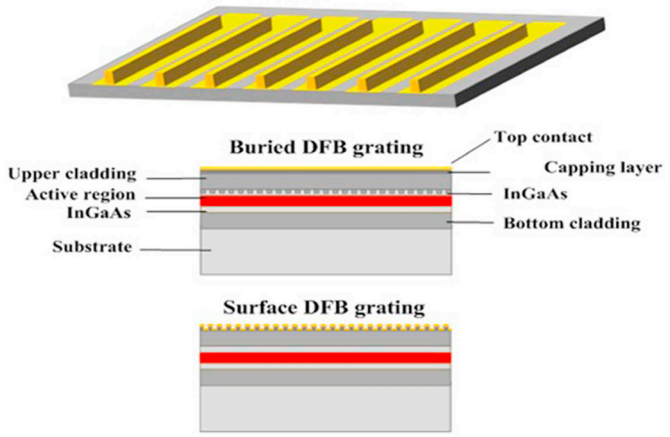

Fig. 11. Distributed feedback QCL (DFB-QCL) array. Middle: buried DFB grating. Bottom: surface DFB grating [96]. Reprinted with permission from ref. 96.

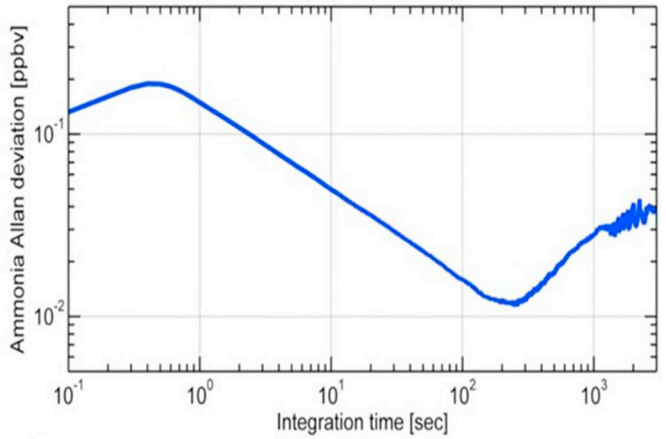

Fig. 12. Allan deviation plot of 14.6 ppbv NH_3 [104]. Reprinted with permission from ref. 104.

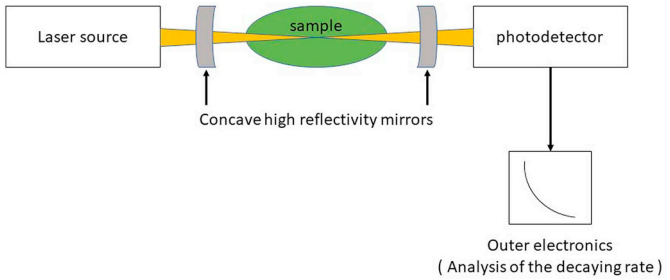

Fig. 13. Scheme of a typical CRDS setup.

compact and portable gas sensor applications. Cavity ringdown spectroscopy (CRDS) is one of the auxiliary methods to reduce the long optimal pathlength required for highly sensitive and selective gas detection in TDLAS. Basically, as depicted in Fig. 13, this technique is based upon the variance between measurements of the decaying rate of laser intensity with and without the presence of the analyte gas [109]. Once a laser beam emits from the source, it passes through the optical cavity (resonator) and the multiple reflections of the beam occur between the reflectors (mirrors). Consequently, the optimal optical path of the radiation up to several kilometers can be obtained and the output signals are collected and processed by the photodetector and the outer electronics, respectively.

Lately, He et al. [110] has achieved detection limits of ~11 ppbv for

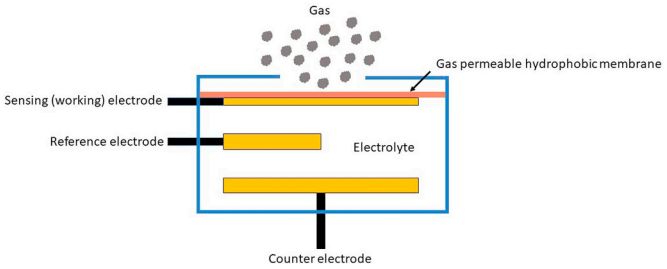

Fig. 14. A basic electrochemical sensor in schematic design.

NH_3 in N_2 and ~300 ppbv for NH_3 in air with their fiber-coupled rapidly swept continuous wave (cw)-CRDS technique. Since the performance of a cw-CRDS system highly relies on the short-term frequency stability of its laser source, they employed external cavity diode lasers (ECDLs) that exhibits superior short-term frequency stability to DFB lasers, yielding ten times better sensitivity than DFB lasers with their system configuration. The distinct advantages of their technique over other CRDS based NH_3 detecting measurements are its docility to utilize a single optical transmitter/receiver console comprised of multiple passive sensor units and the remote monitoring of analyte gases from one or more locations.

5. Other methods

5.1. Electrochemical sensors

This method has been used for gas sensors due to its attractive aspects including lower power consumption, portability, and cost-efficient fabrication as well as high sensitivity and relatively perfect selectivity [111]. Normally, as shown in Fig. 14, a typical electrochemical gas sensor consists of a sensing electrode (or working electrode), a counter electrode, a reference electrode, an electrolyte and a gas permeable hydrophobic membrane (usually PTFE or Teflon) [12,112].

Generally, in this sensor category, the sensors sorted as types of electrolyte and, solid and liquid state electrolytes are utilized the most. More specifically, the solid-state electrolyte-based sensors normally use amperometric and potentiometric techniques and, on the other hand, the liquid state electrolyte sensors usually employ voltammetric and potential step chronoamperometric methods [113]. The NH_3 gas sensors using potentiometric method, for example, adopt a sensing mechanism that the difference in the electrical potential between the sensing and counter electrodes is measured when NH_3 gas diffuses across the gas permeable membrane into the electrolyte solution, and the electrochemical reaction between the electrolyte and NH_3 gas molecules occurs at the sensing electrode [114–116]. As a result of the electrochemical reaction, nitrogen, hydrogen ions and six electrons are produced through oxidation of ammonia at the sensing electrode and, meanwhile water is formed at the counter electrode through the reaction between hydrogen ions generated from the sensing electrode and oxygen as follow:

$$2NH_3 \rightarrow N_2 + 6H^+ + 6e^- \quad (9)$$

$$O_2 + 4H^+ + 4e^- \rightarrow 2H_2O \quad (10)$$

This type of sensor is greatly dependent on the function of electrolyte and, namely, the electrolyte plays a very important role in sensor performance. Therefore, most shortcomings come with the malfunction of electrolyte. For instance, liquid electrolyte-based sensors suffer from the fact that a significant amount of electrolyte is consumed for each detection and the total lifespan of the sensor reduces as the amount of liquid electrolyte in the sensor decreases [111,117]. In the case of solid electrolyte-based sensors, it suffers from the possibility of electrolyte poisoning and its application is limited due to the relatively high required operation temperature (> 200°) [117].

Table 2
A list of ionic liquids used in gas sensors. Regenerated from ref. [126].

Acronym	Name of the ionic liquid
$[C_2MIM][NTf_2]$	1-ethyl-3-methyl-imidazolium bis(trifluoromethyl-sulfonyl)imide
$[C_3MIM][NTf_2]$	1-propyl-3-methyl imidazolium bis(trifluoromethyl-sulfonyl)imide
$[C_4MIM][NTf_2]$	1-butyl-3-methyl imidazolium bis(trifluoromethyl-sulfonyl)imide
$[C_6MIM][NTf_2]$	1-hexyl-3-methyl imidazolium bis(trifluoromethyl-sulfonyl)imide
$[C_8MIM][NTf_2]$	1-octyl-3-methyl imidazolium bis(trifluoromethyl-sulfonyl)imide
$[C_{10}MIM][NTf_2]$	1-decyl-3-methyl imidazolium bis(trifluoromethyl-sulfonyl)imide
$[C_2MIM][PF_6]$	1-ethyl-3-methyl-imidazolium hexafluorophosphate
$[C_4MIM][PF_6]$	1-butyl-3-methyl-imidazolium hexafluorophosphate
$[C_6MIM][PF_6]$	1-hexyl-3-methyl-imidazolium hexafluorophosphate
$[C_8MIM][PF_6]$	1-octyl-3-methyl-imidazolium hexafluorophosphate
$[C_2MIM][BF_4]$	1-ethyl-3-methyl-imidazolium tetrafluoroborate
$[C_4MIM][BF_4]$	1-butyl-3-methyl-imidazolium tetrafluoroborate
$[C_6MIM][BF_4]$	1-hexyl-3-methyl-imidazolium tetrafluoroborate
$[C_8MIM][BF_4]$	1-octyl-3-methyl-imidazolium tetrafluoroborate
$[C_4MIM][Ac]$	1-butyl-3-methyl-imidazolium acetate
$[C_4MIM][OTf]$	1-butyl-3-methyl-imidazolium trifluoromethanesulfonate
$[C_4MIM][NO_3]$	1-butyl-3-methyl-imidazolium nitrate
$[C_4MIM][C(CN)_3]$	1-butyl-3-methyl-imidazolium tricyanomethyl
$[C_4MIM][N(CN)_2]$	1-butyl-3-methyl-imidazolium dicyanamide
$[C_6MIM][Cl]$	1-hexyl-3-methyl-imidazolium chloride
$[C_5MIM][FAP]$	1-pentyl-3-methyl-imidazolium trifluorotris-(pentafluoroethyl) phosphate
$[C_6MIM][FAP]$	1-hexyl-3-methyl-imidazolium trifluorotris-(pentafluoroethyl) phosphate
$[C_4DIM][NTf_2]$	1-butyl-2,3-dimethyl-imidazolium bis (trifluoromethyl-sulfonyl)imide
$[C_4MPY][NTf_2]$	1-butyl-1-methyl-pyrrolidinium bis (trifluoromethyl-sulfonyl)imide
$[N_{6222}][NTf_2]$	hexyltriethylammonium bis(trifluoromethyl-sulfonyl)imide
$[N_{4441}][NTf_2]$	tributylmethylammonium bis(trifluoromethyl-sulfonyl)imide
$[P_{14,666}][FAP]$	trihexyltetradecylphosphonium trifluorotris-(pentafluoroethyl) phosphate
$[P_{14,666}][NTf_2]$	Trihexyltetradecylphosphonium bis(trifluoromethyl-sulfonyl)imide
$[P_{14,666}][AQS]$	Trihexyltetradecylphosphonium 9,10-anthraquinone-1-sulfonate

As aforementioned, electrochemical gas sensors have suffered from the serious drawbacks mostly originating from the electrolyte. Miscellaneous materials for replacement of traditional electrolytes have been studied and exploited to address the issues [113] and, amongst them, the room temperature ionic liquids (RTILs) have been prevalently utilized [118–125]. Basically, RTILs are derived from ionic liquids (ILs) that can be defined as which salts composed of a large organic cation and a much smaller organic or inorganic anion are able to maintain its liquid state below 100°C with only ionic property [126]. In the case of RTILs, it is entirely composed of ions and remains liquid around 298K and below [124]. The ILs including RTILs used in gas sensor applications are listed in Table 2.

Compared to typical aqueous electrolytes with the range of 1.23 V, not only do RTILs exhibit a superior electrochemical durability range from 4 to 5 V, but they also excel in other electrolyte materials used for electrochemical gas sensor in that it possesses high intrinsic ionic conductivity, negligible vapour pressure, the ability to maintain liquid state at a wide range of temperatures above and below room temperature, high thermal stability, high polarity, high viscosity and wide potential windows [127–129]; however, at the same time, there is also a critical disadvantage of the use of RTILs in electroanalytical measurements, namely its low diffusion coefficients. The fairly high viscosity of RTILs causes slower mass transport of redox species than in traditional aqueous or non-aqueous electrolytes, leading to sluggish diffusion coefficients and, as a result, small current signals [130].

Through improving the diffusion, Oudenhoven et al. [131] demonstrated an enhanced electrochemical NH_3 gas sensor using the RTIL consisting of 1-butyl-3-methylimidazolium bis (trifluoromethyl sulfonyl) imide $[BMIM][NTf_2]$ with a thickness of 5 μm. Due to the general advantages of RTIL and its thin thickness, they were able to accomplish the detection limit of 1 ppm NH_3 under ambient conditions (RT, 40 % RH) as shown in Fig. 15 (b). Additionally, the data comparison was made between amperometry and cyclic voltammetry as their evaluation methods for sensing response towards gaseous NH_3. Consequently, they found that cyclic voltammetry is more viable with their system configuration since low concentrations could be lucidly detected and a diminishing sensitivity during NH_3 exposure does not interrupt sensor operation.

Another prevalent approach to enhance the performance of the electrochemical NH_3 gas sensors is using robust and noble materials as electrodes or substrates in sensor device fabrication. Sekhar et al. [132] has delivered an enhanced electrochemical NH_3 sensor by employing paper as a substrate. In fact, paper-based sensors have been utilized in various application fields, such as food quality control, environmental monitoring and etc., because of its capability either in simple and low-cost fabrication or in portable and disposable device configuration [133–135]. Due to its unique properties such as compatibility with chemicals and passive liquid transport, a paper substrate was selected to build an enhanced paper-based electrochemical NH_3 sensor and the device achieved fast response time (~8s) and recovery time (~7s) as defined as the time consumed for the sensor output to reach 90% of the maximum current and the time consumed for the sensor output to diminish to 10% of the current in measurement, respectively. In addition, the detection limit of 1 ppm was achieved in utilizing their room temperature paper-based NH_3 gas sensor. Furthermore, Liu et al. [136] demonstrated a highly sensitive room temperature NH_3 gas detection by applying noble materials for their electrode fabrication. Due to its higher activity than other single noble metals with respect to electrochemical oxidation of NH_3 in alkaline solution [137–139], the bimetallic Pt-Ir alloy was chosen and prepared onto a porous Al_2O_3 ceramic plate by typical sputtering and electroplating techniques. Consequently, the electrode structure consisting of Pt-Ir alloy, Pt, and the porous ceramic plate (PCP) was constructed as a complete electrode in their reactor for detection of gaseous NH_3 as depicted in Fig. 16 (A). Since they employed the traditional three electrode system, the Pt-Ir/Pt/PCP was adopted as the sensing(working) electrode, and the Pt wire and Pt plate as the counter and reference electrodes, respectively. Prior to the electrochemical measurement, their working electrode was activated at 0.6 V in 1.0 M KOH aqueous solution for 2 h. Additionally, the polarization and chronoamperometric techniques were utilized to monitor the behaviours of NH_3 oxidation on the electrodes and the sensing properties of the amperometric NH_3 sensors, respectively. With their

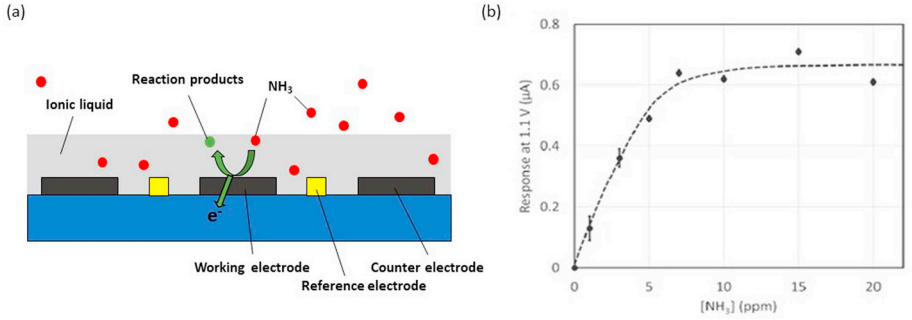

Fig. 15. A schematic representation of the configuration and operating principle of a thin RTIL film based NH_3 gas sensor. Regenerated from ref. 131 (a), voltammetric response measured at 1.1 V as a function of the NH_3 concentration (b) [131]. Reprinted with permission from ref. 131.

electrochemical NH_3 gas sensing system, the detection limit of 2 ppm NH_3 gas was achieved and good response-recovery properties, linear dependence and great repeatability were also obtained. The enhanced sensing properties might be attributed to the stronger adsorption of NH_3 gas on Pt-Ir alloy [140]; however, as shown in Fig. 16 (B), the sensitivity of the device is highly dependent on the humidity and, especially, it escalates as the humidity increases. It might be attributed to the fact that the NH_3 is gradually oxidized into nitrogen or hydrogenated nitrogen on Pt as following equations (Eq. 11–14) in low humidity (0% R.H.) and the adsorbate of N_{ads} would trigger the deactivation of the electrode more than the other adsorbed species (NH_{ads} or $NH_{2,\ ads}$) [136]. On the other hand, under high humidity (98% R.H.), the regenerative reaction between the adsorbed nitrogen (N_{ads}) and the adsorbed hydrogen (H_{as}) is taken place on the surface of the electrode (see Eq. 15–18) [136]. As a result, more adsorption sites would be created as the adsorbate of N_{ads} is consumed for the reaction, resulting in the improved sensitivity of the electrode under the high humid condition.

$$NH_3 + OH^- + Pt \leftrightarrow Pt - NH_2 + H_2O + e^- \quad (11)$$

$$Pt - NH_2 + 2OH^- \leftrightarrow {}^1/_2N_2 + 2H_2O + 2e^- + Pt \quad (12)$$

$$Pt - NH_2 + OH^- \leftrightarrow Pt = NH + H_2O + e^- \quad (13)$$

$$Pt = NH + OH^- \leftrightarrow {}^1/_2N_2 + H_2O + 2e^- + Pt \quad (14)$$

$$H_2O + Pt + e^- \rightarrow Pt - H + OH^- \quad (15)$$

$$Pt - H + Pt \equiv N \rightarrow Pt = NH + Pt \quad (16)$$

$$2Pt - H + Pt \equiv N \rightarrow Pt - NH_2 + 2Pt \quad (17)$$

$$Pt - H + PtH \rightarrow 2Pt + H_2 \quad (18)$$

5.2. Surface acoustic wave (SAW) sensors

The major advantages of SAW gas sensors are ability of real-time detection, low power consumption, high sensitivity, stability in harsh environments, such as high pressure, high temperature, and corrosive conditions, and eligibility in wireless applications [141].

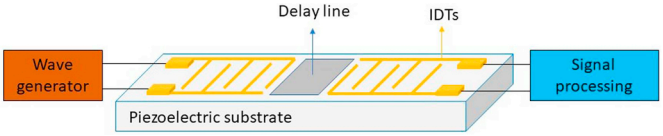

Fig. 17. A schematic design of a SAW device.

A typical configuration of a SAW gas sensor consists of two interdigitated transducers (IDTs) on the piezoelectric substrates, such as quartz, lithium niobate, or langasite with a delay-line between the IDTs as shown in Fig. 17. Usually, the IDTs on the surface of the SAW gas sensors are made of noble metals such as gold or platinum and work as transmitting and receiving transducers for the SAW.

The working principle of a SAW gas sensor employs the detection of a surface variation, also known as surface perturbations, in velocity or amplitude of the wave generated by the reaction between the delay-line and analyte gases. Since the frequency shift is influenced by the mass change of a specific gas, the perturbation theory can be applied to explain how the SAW based NH_3 gas sensor works [142,143],

$$\Delta f \cong (k_1 + k_2) f_0^2 m/A \quad (19)$$

where f_0 is the center frequency of the SAW sensor (Hz), k_1 and k_2 are piezoelectric material constants, m is the mass of NH_3 molecule absorbed on the delay-line, and A is the area of the delay-line. In addition to the perturbation theory, a typical gas sensing mechanism of a SAW sensor is based on a change in the film conductivity that leads to changes in SAW velocity and, consequently, shifts of the central frequency [144,145]. The relationship between the change of SAW velocity (Δv) or the change of central frequency (Δf) versus the surface conductivity (σ_s) of the film is given as [146]:

$$\frac{\Delta f}{f_0} = \frac{\Delta v}{v_0} \approx -\frac{k^2}{2}\frac{\sigma_s^2}{\sigma_s^2 + v_0^2 C_s^2} \quad (20)$$

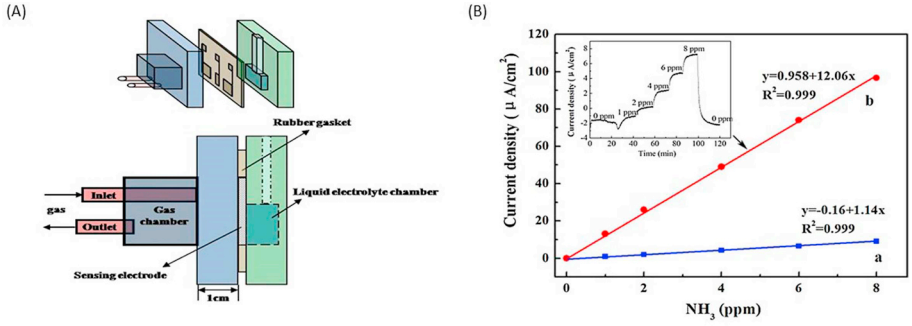

Fig. 16. the schematic diagram of the reactor (A), the response curves to different NH_3 concentrations in (a) 0% and (b) 98% R.H. gas phase (B) [136]. Reprinted with permission from ref. 136.

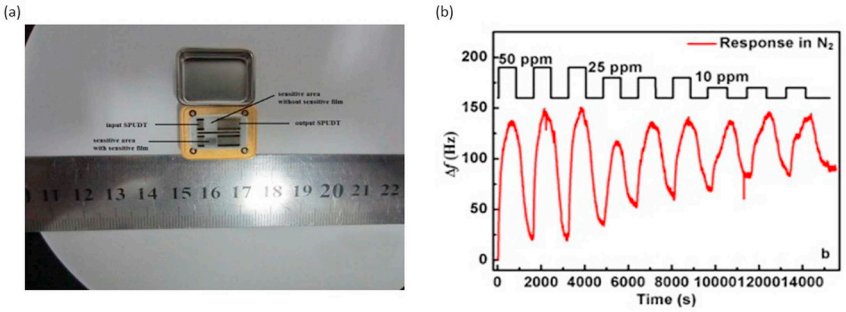

Fig. 18. A picture of SAW NH_3 gas sensor based on Pt doped 2 layered PPy film (a), response of the device to different concentrations of NH_3 in N_2 (b) [149]. Reprinted with permission from ref. 149.

where f_0 is the resonant frequency, v_o is the undisturbed SAW velocity, C_s is the surface capacity and k is an electromechanical coefficient.

Since the delay-line is a critical component of a SAW gas sensor in detecting analyte gases, numerous types of sensing materials including noble metals, metal-oxides, dyes, carbon nanotubes (CNTs) and polymers have been employed as delay-line materials for detection of gaseous NH_3 [147,148].

For enhancement in sensing performance, robust and versatile materials have been explored and employed in SAW gas sensing applications as a sensing element on the delay-line. For instance, Chen et al. [149] demonstrated a highly sensitive RT SAW NH_3 gas sensor with platinum (Pt) doped polypyrrole (PPy) film (see Fig. 18). Although conducting polymers is one of the most frequently used materials in SAW gas sensing application because of their low-cost and RT gas sensing characteristics, it also has suffered from the lack of long term stability and reliability due to degradation of polymer coatings, especially, caused by vapour permeation into the polymer while exposed to analyte gases [150,151]. To address the issue, Chen et al. employed the double layer of PPy with Pt and, consequently, the stability and response of the sensor was improved by the advanced structure of conducting polymer and the catalytic effect of Pt, which leads to the acceleration of reaction between gaseous NH_3 and PPy and the larger electrical loading effect resulting from larger drop of the resistance of PPy as following reactions [152]:

$$Pt + NH_3(gas) \leftrightarrow Pt - NH_2^- - H^+ \quad (21)$$

$$PPy^+ + NH_2^- \leftrightarrow PPy/NH_2 \quad (22)$$

Not surprisingly, semiconducting metal oxides including ZnO, TiO_2, SnO_2, In_2O_3, Fe_2O_3, MoO_3, CuO, NiO and Co_3O_4 have been well recognized as sensing film materials in SAW gas sensor fields [153,154]. For the advanced sensing performance of metal oxide-based SAW sensors, the metal oxide-based composite structures have been widely accepted [155]. For example, Wang et al. [156] claimed an advanced RT SAW NH_3 sensor using the ZnO/SiO_2 composite film on piezoelectric ST-cut quartz substrate. At room temperature, such device could achieve the detection limit of 10 ppm, and 65 s and 60 s as the response and recovery times, respectively. By the sol-gel spin coating method with the optimized molar ratio of 1:2 (ZnO: silica), they were able to prepare the ZnO/SiO_2 composite film and improve the film sensitivity towards NH_3 at RT in terms of the increase of the film conductivity, comparing to that of the pristine ZnO film (see Fig. 19). The rise of the film conductivity might be attributed to the fully hydroxylated SiO_2 surface caused by a mass of dangling Si bands on the surface and water absorption onto the hydroxyl groups. As a result, due to its high solubility in water, more NH_3 molecules were seized by the absorbed water on the surface and oxidized as releasing more electrons to the conduction band, which leaded to the increase of the film conductivity. Furthermore, the NH_4^+ produced from the reaction between NH_3 and water molecules on the surface might generate a significant increase in surface conductivity, resulting in the enhanced sensitivity.

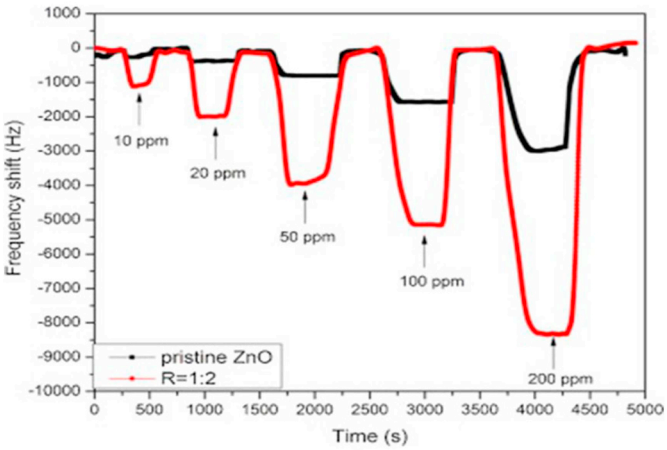

Fig. 19. Sensor responses of the ZnO/SiO_2 composite and pristine ZnO films to different concentrations of NH_3 in air at room temperature [156]. Reprinted with permission from ref. 156.

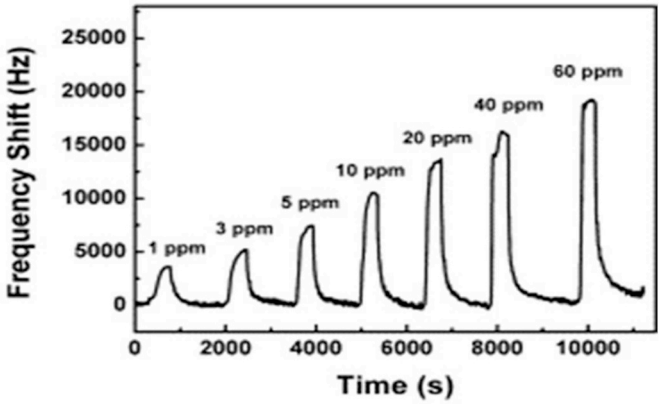

Fig. 20. Sensor response of the quartz SAW NH_3 sensor based on Co_3O_4/SiO_2 composite film at RT [157]. Reprinted with permission from ref. 157.

Similarly, Tang et al. [157] demonstrated the enhanced Co_3O_4/SiO_2 composite sensing film by a sol-gel process onto the ST-cut quartz SAW resonators. With the optimized Co/(Si + Co) molar ratio of 0.5, this device was able to reach the detection limit of 1 ppm (Fig. 20) and possessed decent selectivity and stability.

The role of SiO_2 in the performance enhancement of this device was critical since the presence of SiO_2 can generate a large number of H_2O molecules on the surface of Co_3O_4/SiO_2 composite film and lead to an improved response with respect to the increase of the film conductance. Once the colloidal silica film reacted with NH_3, siloxane bonds were produced by a condensation mechanism between SiO^- species and other

neutral silicate species. As a consequence, a lot of H_2O molecules were gained on the surface of the colloidal silica film, leading to the rise of the film conductance. In addition, the more H_2O molecules that exist on the surface, the more NH_3 molecules can be absorbed on it. Therefore, more electrons that were produced from the oxidation of the NH_3 molecules were released to the conduction band and increased the film conductivity, which leaded to the enhancement of the sensor performance in NH_3 gas detection.

5.3. Field-effect transistor (FET) sensors

Basically, this type of sensor adopts the basic structure of a metal-insulator-semiconductor (MIS) junction and measures the change in the *I-V* (current-voltage) characteristics of the device induced by the presence of a specific analyte for gas sensing [158–160]. Particularly, the metal-oxide-semiconductor field-effect transistor (MOSFET) model is commonly employed in this type of gas sensor.

As a critical component in the MOSFET gas sensor, the gate consists of a gas sensitive film that is typically made up of catalytic metals, such as platinum, palladium, Iridium, etc. and the selectivity of this type of gas sensors highly depends on the electric characteristics of those catalytic metals; however, recently, another catalytic material such as a metal oxide or a conducting polymer is also frequently applied [160]. For NH_3 gas sensing, platinum, palladium, Iridium or mixtures of those metals have been generally utilized and their physical properties, such as a film thickness, structure, or morphology, play an important role with regard to high NH_3 sensitivity [160]. Especially, a porous film is preferable so that the triple points of the metal, insulator (oxide) and NH_3 gas can be well formed in the porous structure of film [159]. Moreover, it facilitates the dissociation of hydrogen atoms from the NH_3 molecules which leads to the diffusion of the hydrogen atoms to the metal-insulator interface or the spill-over to the oxide. As a result, a polarized dipolar layer is formed predominantly at the metal-insulator interface and the magnitude change of the dipoles is caused by the concentration variance of NH_3 gas, which leads to the negative shifts of the threshold potential. The change in sensor signal is measured as the ratio of change in drain current and also called the sensor response (S) defined as [159,161]:

$$S = \frac{I_{DS(air)} - I_{DS(NH_3)}}{I_{DS(air)}} \times 100\% \quad (23)$$

$$I_{DS} = \left(\frac{WC_i}{2L}\right)\mu(V_{GS} - V_T)^2 \quad (24)$$

where $I_{DS\ (NH3)}$ and $I_{DS\ (air)}$ are the drain saturation currents under NH_3 and air environments, respectively, C_i is the capacitance per unit area of an insulator, W is the channel width, L is the channel length, μ is the field effect mobility, and V_{GS} is the gate voltage, and V_T is the threshold voltage (see Fig. 21).

The major advantages of FET NH_3 gas sensor are low power consumption in ambient conditions and cost-efficient production; however, the relatively high operation temperature (100 ~ 300°C) is normally

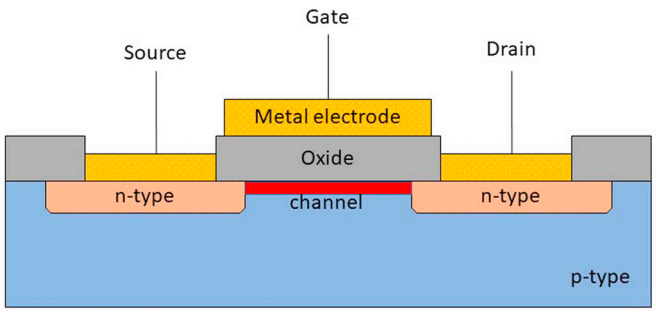

Fig. 21. Schematic configuration of a typical MOSFET gas sensor.

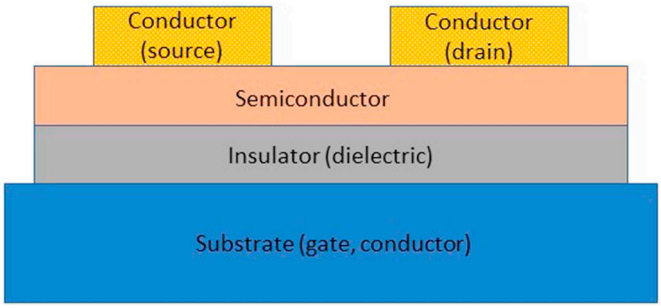

Fig. 22. Typical structure of an organic field effect transistor.

required for an accurate measurement since the pre-adsorbed species, such as water or hydrocarbons, disturb the sensing process severely at room temperature [162].

Many attempts have been made to enhance the FET-based NH_3 sensors. Amongst them, the research into organic field-effect transistor (OFET) NH_3 sensors has intensified due to its flexibility, potential high sensitivity, low cost, light weight, and potential in mass production that are promising aspects in portable sensing systems [163,164]. Similar to MOSFETs, OFETs also consist of three major terminals, the gate, source, and drain, as well as a semiconductor layer and an insulating layer between the semiconductor and gate as shown in Fig. 22. However, it is different from MOSFETs in that an ion-conducting organic dielectric material is used as an insulator and an electrical response can be detected when an analyte contacts the conductive channel located at the interface between an organic semiconductor (OSC) and a dielectric [165–167]. Generally, the p-type OFET is much more common than the n-type one because of its high hole mobility that is directly related to the performance of the sensor [168]. For improving sensing performance, lateral scaling (microstructuring) and vertical scaling (thinning) of OSC thin film and the material selection for sensing film have been considered and explored in the field of OFET based NH_3 gas sensors so as to accelerate the interaction between analytes and the conductive channel as a critical parameter in determining sensing performance [169–175].

Besar [172] and Kumar et al. [173] reported advanced OFET based NH_3 gas sensors using poly (3, 3‴-didodecylquarterthiophene) (PQT-12) as an active semiconducting film that has excellent sensitivity to NH_3 [176]. The sensing mechanism of NH_3 gas on the PQT-12 film can be described with respect to chemical interaction between NH_3 and PQT-12 causing dedoping in the polymer chain [177]. Under the condition of absence of NH_3, when the negative voltage is applied to the gate of OFET sensor, the conducting channel is formed by the accumulation of majority positive charges (holes) at the polymer-dielectric interface. Once the sensing film is exposed to NH_3 gas, the lone pair of electrons in NH_3 gas start interacting with PQT-12 and the net positive charges (holes) of the polymer are reduced, which results in the reduction in hole concentration along with the decrease of the drain current. During recovery with air, the NH_3 gas with the lone pair of electrons begins to discard from the PQT-12 chain and the polymer returns to its initial stable molecular structure [172,173].

According to Besar et al., the significantly simple OFET structure could be accomplished by using PET substrate as gate dielectric and corona-induced charging treatment that creates a sole source of electric field and facilitates easy manipulation in OFET characteristics, such as threshold voltage [178–180]. As a result, they were able to achieve a low detection limit of 100 ppb by measuring the percentage change in the drain current as mentioned in Eq. (23). Although the decent sensing performance was obtained with its compact OFET structure and the NH_3 sensitive PQT-12 film, it should be addressed that the decay of the charges resulting from desorption or migration with time causes the performance instability and high voltage is required for device operation because of its mediocre mobility under low voltages (see Fig. 23).

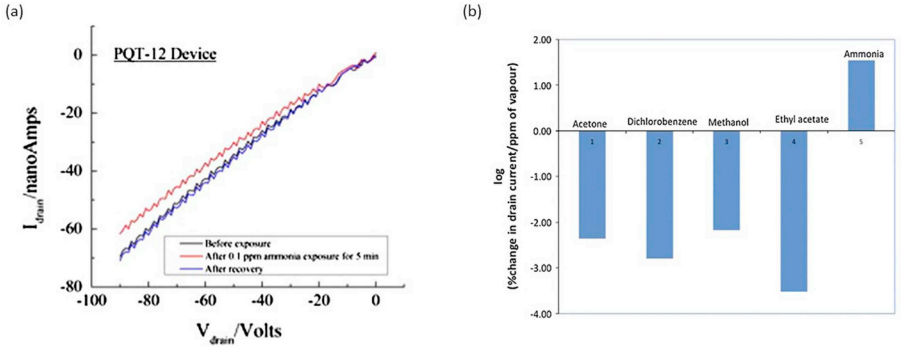

Fig. 23. Response to 100 ppb of ammonia in *I-V* plot (a), responses expressed as log percent change of current per ppm of analyte gases (b) [172]. Reprinted with permission from ref. 172.

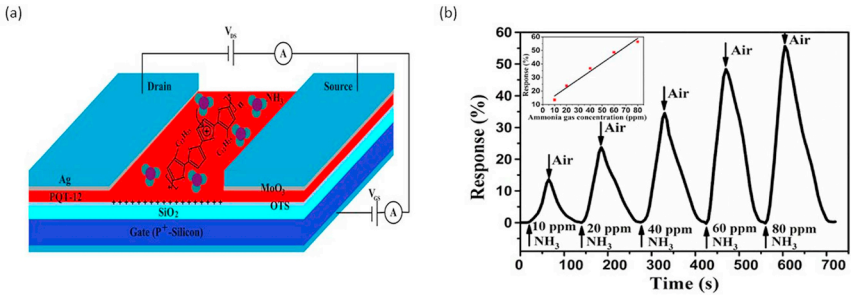

Fig. 24. NH_3 gas interaction mechanism in as-fabricated OFET sensor (a), transient response of FTM coated OFET sensor for various concentration of NH_3 gas (b). Inset: response curve from 10 to 80 ppm of NH_3 [173]. Reprinted with permission from ref. 173.

On the other hand, Kumar et al. suggested a sophisticated film fabrication method that is the floating film transfer method (FTM) whose advantages are simplicity and cost-effectiveness in fabrication [181]. It is noted that the film thickness of PQT-12 influences the charge transport phenomenon between source and drain of the OFET, and the increased PQT-12 film thickness increases the drain current of the OFET sensor, resulting in the decrease of the sensor response [182,183]. Therefore, a thin PQT-12 film of ~20 nm fabricated by the FTM played an important role in enhancing the sensing performance and the device represented enhanced sensing properties as the response time and recovery time of ~45 s and ~85 s, respectively. A low detection limit of 404 ppb was also achieved (see Fig. 24).

Moreover, Yu et al. [184] demonstrated a high-performance polymer transistor-based NH_3 gas sensor in using poly (2,5-bis (3-tetradecylthiophen-2-yl) thieno [3,2-b] thiophene) (PBTTT) as a sensing semiconducting polymer and OTS-modified SiO_2 as a substrate. The enhanced sensing performance of their system might be attributed to its nanostructured polymer semiconductor (PBTTT) that enables to maintain the high charge carrier mobility, which is a critical aspect in advanced OFET-based gas sensors [185,186]. The charge carrier mobility determines the signal transfer speed that is related to the sensor response time and recovery time, and the relation between the charge carrier mobility and the transit time is defined as the following equation [187]:

$$t = \frac{L^2}{V\mu} \tag{25}$$

where L is the channel distance, V is the applied voltage, and μ is the charge carrier mobility. The large two-dimensional crystalline domains in their PBTTT film provide a high surface area and optimal percolation pathways for charge carriers. Consequently, the response time of a few seconds and the recovery time of ~10 s, and the detection limit of 10 ppm were achieved with the PBTTT transistor-based NH_3 gas senor.

6. Summary

Recently reported NH_3 gas sensors utilizing advanced detecting techniques that are discussed in this review are summarized in Table 3. As shown in the table, metal oxide based NH_3 sensors using structural manipulation or hybridization with other sensing materials are able to achieve superior sensing performances to others utilizing solely metal oxides when it comes to the lowest detection limit, fast response and recovery times, and operability in room-temperature. For instance, the SnO_2 nanoparticle-coated In_2O_3 nanofiber structure represents the highest sensitivity of 100 ppb and fast response and recovery times of 7 s and 10 s, respectively, at room-temperature. The hybridization strategy has been also widely adopted in polymer based NH_3 gas sensors to improve its sensing characteristics and, especially, the PANI-based system with a PU matrix exhibits the lowest detection limit of 20 ppb in its group of detecting method; however, the fastest response time of 7 s is achieved by PANI nanocomposites doped with Cu nanoparticles. Since it has been well known as one of the most highly sensitive and selective NH_3 gas detectors, TDLAS with integration of multiple open-path QCL enables to detect the lowest NH_3 concentration of 150 pptv, comparing to any other NH_3 gas sensing techniques introduced in this review. For the electrochemical method, a paper-substrate based NH_3 gas sensor using RTIL can achieve 8 s and 7 s as its response and recovery times, respectively, with a relatively low detection limit of 1 ppm, which is the most impressive sensing performance in its category. The wide range of capability of incorporation with other sensing materials such as metal oxides, conducting polymers, and nanocomposites is the most attractive aspect of the SAW gas sensor and, for example, the ST-cut quartz SAW resonator with the enhanced Co_3O_4/SiO_2 composite sensing film shows the most remarkable sensing performance in the SAW based NH_3 sensors as the detection limit of 1 ppm and the response time of 35 s at room-temperature. In the FET type of NH_3 detectors, OFET based NH_3 gas sensors using PQT-12 represent the most outstanding sensitivity as low as 100 ppb

Table 3
Sensing performance of the recently reported NH_3 gas sensors in advanced techniques.

Sensing Methods	Detection limit	Response time	Recovery time	Operation temperature	Reference
Metal oxide					
SnO_2/Pd/RGO	2 ppm	7min	50min	RT	[46]
SnO_2/In_2O_3	100 ppb	7s	10s	RT	[47]
SnO_2/Co_3O_4	5 ppm	4s	17s	200°C	[51]
TiO_2	5 ppm	34s	90s	RT	[191]
SnO_2/Sr	10 ppm	6s	-	RT	[192]
ZnO/NiO	15 ppm	20s	90s	RT	[193]
ZnO/Pd	30 ppm	198s	334s	200°C	[194]
NiO/In_2O_3	100 ppb	-	-	300°C	[195]
SnO_2/rGO	20 ppm	8s	13s	RT	[196]
TiO_2/graphene	5 ppm	114s	304s	RT	[197]
ZnO/Mn	20 ppm	4s	10s	150°C	[198]
$NiCo_2(OH)_6$	2 ppm	28s	20s	RT	[199]
$NiCo_2O_4$	2 ppm	30s	13s	RT	
ZnO/MoS_2	250 ppb	10s	11s	RT	[2000]
Conducting polymer					
PANI/ZnO	25 ppm	-	-	RT	[16]
PANI/TSA	5ppm	10s	100s	RT	[70]
PVDF-PANI(DBSA)	100 ppb	2.5min	-	RT	[71]
PBuA-PANI(HCl)	250 ppb	2.5min	-	RT	
PU-PANI(CSA)	20 ppb	5min	-	RT	
PANI/Cu	1 ppm	7s	160s	RT	[76]
PANI	5 ppm	213s	98s	RT	[173]
PANI/graphene	1 ppm	50s	23s	RT	[201]
PEDOT:PSS/MWCNT	1 ppm	15min	20min	RT～150°C	[202]
PANI/ZnO	10 ppm	-	-	RT	[203]
TDLAS					
QCL	150 pptv	-	-	40°C	[106]
DFB-QCL	6 ppb	1s	-	RT	[107]
ECDLs/cw-CRDS	11 ppbv	-	-	RT	[110]
DFB-QCL	14.6 ppbv	2s	-	RT	[204]
Electrochemical					
RTIL	1 ppm	10s	-	RT	[131]
RTIL	1 ppm	8s	7s	RT	[132]
$H_2PtCl_6/IrCl_3$	2 ppm	7min	11.2min	RT	[136]
SAW					
ZnO/SiO_2	5 ppm	38s	30s	RT	[146]
Pt doped PPy	10 ppm	-	-	RT	[149]
ZnO/SiO_2	10 ppm	65s	60s	RT	[156]
Co_3O_4/SiO_2	1 ppm	35s	100s	RT	[157]
FET					
Pentacene	10 ppm	5min	50min	-	[165]
Poly(3-hexylthiophene)(P3HT)	383 ppb	-	-	RT	[169]
PC_{61}BM-P3HT	186 ppb	5min	20min	RT	
P3HT-PC_{61}BM	259 ppb	4min	20min	RT	
P3HT/PC_{61}BM	298 ppb	3min	9min	RT	
P3HT/polystyrene	5 ppm	-	-	-	[170]
PQT-12	100 ppb	-	-	-	[172]
PQT-12	404 ppb	45s	85s	RT	[173]
Pentacene/PVA	200 ppb	-	-	-	[175]

and the quickest response and recovery times as 45 s and 85 s, respectively.

7. Concluding remarks

A great number of different sensing methods for NH_3 gas detection have been extensively investigated in last decades to alleviate the concerns over the environment and the public health. Among the frequently utilized NH_3 gas sensing methods, solid state sensing techniques including metal oxide and conducting polymer-based sensors have occupied a substantial portion of NH_3 gas sensor applications due to its outstanding advantages over other sensing methods, such as simple and cost-effective fabrication and decent compatibility with other materials for synergistic effects in sensing performance. Especially, metal oxide based NH_3 gas sensors have been intensely studied and widely applied because of its intrinsic high sensitivity towards NH_3 gas. However, a lot of efforts are still needed to improve its selectivity towards NH_3 gas. Moreover, most metal oxide-based NH_3 gas sensors require relatively high temperature, which is not promising in terms of energy efficient operation, portability, real-time detection, etc. Currently, one of advanced approaches to address these issues is the incorporation with carbon nanomaterials [188]. Specifically, carbon nanotube (CNT) or layered graphene is utilized to reduce the operation temperature due to its high electron mobility that is capable of improving the typical sluggish recovery rate of metal oxides greatly; however, with regard to the room temperature operation, it still needs to be developed that lower desorption rate of analyte gases at room temperature and the high adsorption energy between analyte gas molecules and the active areas in sensing materials preclude the rapid recovery back to its initial state. Therefore, the future research in metal oxide based NH_3 gas sensors should be focusing on the enhancement in either selectivity or room temperature operation. Similar to metal oxide based NH_3 gas sensors, conducting polymer based NH_3 gas sensors have also suffered from low selectivity resulting from humidity and swelling effect in conducting polymer sensing layers. In fact, humidity in air and swelling effect are merely minor drawbacks and the main shortcomings result from irreversibility and long-term instability. Although the mechanism of irreversibility has not been clearly explained in literature, it might be

attributed mainly to nucleophilic attack on carbon backbone [189]. Additionally, the long-term stability is hardly obtained due to the de-doping phenomenon in conducting polymers. Therefore, the improvement in the reversibility and long-term stability of conducting polymer based NH_3 gas sensors could be a future research orientation. Generally, to satisfy a high degree of sensitivity and selectivity, the complexed configuration of sensing system in TDLAS is required, leading to the high cost in system build-up. Moreover, the device miniaturization could also be hampered by the sophisticated system configuration. Although there have been attempts utilizing novel and advanced laser sources or spectroscopy to overcome these drawbacks, exploring new laser sources and developing spectroscopic techniques should be conducted as a future research subject for the enhanced TDLAS based NH_3 gas detection. As aforementioned, the RTILs have been widely employed to address the major issues caused by the typical electrolytes in electrochemical gas sensors; however, due to its high viscosity and relatively low conductivity, the use of RTILs in electrochemical NH_3 gas sensing has encountered the limitation. One of the suggested solutions so as to compensate the unfavorable properties of RTILs is using new electrode configurations. Micro-electrodes, for example, feature superb signal-to-noise ratio, high mass transport rates, and low uncompensated resistances, which are beneficial to enhance the sensing performance of RTILs based electrochemical NH_3 gas sensors [62,111]. Majority of research efforts so far have been made only on the applications of SAW NH_3 gas sensor, leading to a lack of fundamental studies and comprehensive understanding in sensing mechanisms of the delay-line materials. Therefore, it is expected that more endeavor in understanding physical and electrical properties of sensing materials for the advanced delay-line will be devoted to improve the sensing performance of the SAW NH_3 gas sensors in the future. As has been mentioned, p-type OFET based gas sensors have been predominantly utilized in the field of FET based NH_3 gas detection as an advanced sensing method, which could be considered as there are plenty of space for future research in n-type OFET based NH_3 gas detection. In modern circuitry, both p-type and n-type transistors are embedded together to better detect an analyte gas and, therefore, if impediments in n-type OFETs are surmounted, the significant improvement in sensing performance could be envisaged. With respect to a major concern in utilizing the n-type OFETs, the instability of radical anions under air sufficient condition is generally discussed. There are several suggestions to address this issue and, amongst them, a logically accepted approach is to add functional groups with high electron affinity into p-type semiconducting materials used in the n-type and p-type hybridization gas sensing system, resulting in alleviation of the air instability [190].

To conclude, although a large number of studies in the past mainly focused on the development of single sensing methods for NH_3 gas detection, most of the recent or advanced sensing techniques have accepted the hybridization of either sensing materials or detecting methods. As a field of novel hybridizations across sensing substances or detection techniques for the accurate measurement of NH_3 gas detection has been rapidly growing, further research in the fundamental studies for better understanding of sensing mechanisms, sensing properties, etc. of the sophisticated sensing systems is highly demanded to establish a guideline for improving the sensing performance in NH_3 gas detection. In addition, since selectivity is the most challenging object for nearly all types of NH_3 gas sensors, an increased research endeavor on the enhancement of selectivity in the hybridized NH_3 gas sensing systems will be also required in the future.

Acknowledgement

We thank the financial support from DOE (DE-FE0026219) and Health eSense.

References

[1] N. Tamaekong, C. Liewhiran, A. Wisitsoraat, S. Phanichphant, Flame-spray-made undoped zinc oxide films for gas sensing applications, Sensors 10 (2010) 7863–7873, https://doi.org/10.3390/s100807863.
[2] A.G. Shrivas, R.G. Bavane, A.M. Mahajan, Electronic nose: a toxic gas sensor by polyaniline thin film conducting polymer, Proc. 14th Int. Work. Phys. Semicond. Devices, IWPSD, Mumbai, India, 2007, pp. 621–623 https://www.scopus.com/inward/record.url?eid=2-s2.0-49749130902&partnerID=40&md5=e60c84d1b8b1dc9f0c11000fbe0f1bf0.
[3] S.J. Kim, I.S. Hwang, Y.C. Kang, J.H. Lee, Design of selective gas sensors using additive-loaded In2O3 hollow spheres prepared by combinatorial hydrothermal reactions, Sensors 11 (2011) 10603–10614, https://doi.org/10.3390/s111110603.
[4] I.C. Chen, S.S. Lin, T.J. Lin, C.L. Hsu, T.J. Hsueh, T.Y. Shieh, The assessment for sensitivity of a NO2 gas sensor with ZnGa2O4/ZnO core-shell nanowires-a novel approach, Sensors 10 (2010) 3057–3072, https://doi.org/10.3390/s100403057.
[5] A. Fuerte, R.X. Valenzuela, M.J. Escudero, L. Daza, Ammonia as efficient fuel for SOFC, J. Power Sources 192 (2009) 170–174, https://doi.org/10.1016/j.jpowsour.2008.11.037.
[6] L. Zhang, W. Yang, Direct ammonia solid oxide fuel cell based on thin proton-conducting electrolyte, J. Power Sources 179 (2008) 92–95, https://doi.org/10.1016/j.jpowsour.2007.12.061.
[7] A. Chellappa, C. Fischer, W. Thomson, Ammonia decomposition kinetics over Ni-Pt/Al2O3 for PEM fuel cell applications, Appl. Catal. Gen. 227 (2002) 231–240.
[8] T. Hejze, J.O. Besenhard, K. Kordesch, M. Cifrain, R.R. Aronsson, Current status of combined systems using alkaline fuel cells and ammonia as a hydrogen carrier, J. Power Sources 176 (2008) 490–493, https://doi.org/10.1016/j.jpowsour.2007.08.117.
[9] M. Comotti, S. Frigo, Hydrogen generation system for ammonia-hydrogen fuelled internal combustion engines, Int. J. Hydrogen Energy 40 (2015) 10673–10686, https://doi.org/10.1016/j.ijhydene.2015.06.080.
[10] R. Lan, J.T.S. Irvine, S. Tao, Ammonia and related chemicals as potential indirect hydrogen storage materials, Int. J. Hydrogen Energy 37 (2012) 1482–1494, https://doi.org/10.1016/j.ijhydene.2011.10.004.
[11] G.K. Mani, J.B.B. Rayappan, Selective detection of ammonia using spray pyrolysis deposited pure and nickel doped ZnO thin films, Appl. Surf. Sci. 311 (2014) 405–412, https://doi.org/10.1016/j.apsusc.2014.05.075.
[12] S. Giddey, S.P.S. Badwal, A. Kulkarni, Review of electrochemical ammonia production technologies and materials, Int. J. Hydrogen Energy 38 (2013) 14576–14594, https://doi.org/10.1016/j.ijhydene.2013.09.054.
[13] B. Timmer, W. Olthuis, A. Van Den Berg, Ammonia sensors and their applications - a review, Sensor. Actuator. B Chem. 107 (2005) 666–677, https://doi.org/10.1016/j.snb.2004.11.054.
[14] G.K. Mani, J.B.B. Rayappan, A highly selective and wide range ammonia sensor - nanostructured ZnO:Co thin film, Mater. Sci. Eng. B 191 (2015) 41–50, https://doi.org/10.1016/j.mseb.2014.10.007.
[15] G.K. Mani, J.B.B. Rayappan, A highly selective room temperature ammonia sensor using spray deposited zinc oxide thin film, Sensor. Actuator. B Chem. 183 (2013) 459–466, https://doi.org/10.1016/j.snb.2013.03.132.
[16] V. Talwar, O. Singh, R.C. Singh, ZnO assisted polyaniline nanofibers and its application as ammonia gas sensor, Sensor. Actuator. B Chem. 191 (2014) 276–282, https://doi.org/10.1016/j.snb.2013.09.106.
[17] C.A. Skjøth, C. Geels, The effect of climate and climate change on ammonia emissions in Europe, Atmos. Chem. Phys. 13 (2013) 117–128, https://doi.org/10.5194/acp-13-117-2013.
[18] M.A. Sutton, J.W. Erisman, F. Dentener, D. Möller, Ammonia in the environment: from ancient times to the present, Environ. Pollut. 156 (2008) 583–604, https://doi.org/10.1016/j.envpol.2008.03.013.
[19] K. Sawicka, P. Gouma, S. Simon, Electrospun biocomposite nanofibers for urea biosensing, Sensor. Actuator. B Chem. 108 (2005) 585–588, https://doi.org/10.1016/j.snb.2004.12.013.
[20] A.K. Prasad, P.I. Gouma, D.J. Kubinski, J.H. Visser, R.E. Soltis, P.J. Schmitz, Reactively sputtered MoO3 films for ammonia sensing, Thin Solid Films 436 (2003) 46–51, https://doi.org/10.1016/S0040-6090(03)00524-8.
[21] P. Gouma, K. Kalyanasundaram, X. Yun, M. Stanaćević, L. Wang, Nanosensor and breath analyzer for ammonia detection in exhaled human breath, IEEE Sens. J. 10 (2010) 49–53, https://doi.org/10.1109/JSEN.2009.2036050.
[22] L. Tabrizi, H. Chiniforoshan, High-performance room temperature gas sensor based on gold(III) pincer complex with high sensitivity for NH3, Sensor. Actuator. B Chem. 245 (2017) 815–820, https://doi.org/10.1016/j.snb.2017.01.193.
[23] J. Huang, J. Wang, C. Gu, K. Yu, F. Meng, J. Liu, A novel highly sensitive gas ionization sensor for ammonia detection, Sensors Actuators A Phys 150 (2009) 218–223, https://doi.org/10.1016/j.sna.2009.01.008.
[24] Y.M. Zhao, Y.Q. Zhu, Room temperature ammonia sensing properties of W18O49 nanowires, Sensor. Actuator. B Chem. 137 (2009) 27–31, https://doi.org/10.1016/j.snb.2009.01.004.
[25] G. Wang, Y. Ji, X. Huang, X. Yang, P.I. Gouma, M. Dudley, Fabrication and characterization of polycrystalline WO3 nanofibers and their application for ammonia sensing, J. Phys. Chem. B 110 (2006) 23777–23782, https://doi.org/10.1021/jp0635819.

[26] A.K. Prasad, P.I. Gouma, D.J. Kubinski, J.H. Visser, R.E. Soltis, P.J. Schmitz, Reactively sputtered MoO3 films for ammonia sensing, Thin Solid Films 436 (2003) 46–51, https://doi.org/10.1016/S0040-6090(03)00524-8.
[27] H.J. Kim, J.H. Lee, Highly sensitive and selective gas sensors using p-type oxide semiconductors: Overview, Sensor. Actuator. B Chem. 192 (2014) 607–627, https://doi.org/10.1016/j.snb.2013.11.005.
[28] G. Korotcenkov, Metal oxides for solid-state gas sensors: what determines our choice? Mater. Sci. Eng. B Solid-State Mater. Adv. Technol. 139 (2007) 1–23, https://doi.org/10.1016/j.mseb.2007.01.044.
[29] C. Wang, L. Yin, L. Zhang, D. Xiang, R. Gao, Metal oxide gas sensors: sensitivity and influencing factors, Sensors 10 (2010) 2088–2106, https://doi.org/10.3390/s100302088.
[30] V.E. Henrich, P.A. Cox, The Surface Science of Metal Oxides, 1st pbk, Cambrige University press, 1996.
[31] N. Barsan, D. Koziej, U. Weimar, Metal oxide-based gas sensor research: how to? Sensor. Actuator. B Chem. 121 (2007) 18–35, https://doi.org/10.1016/j.snb.2006.09.047.
[32] S.P. Ghosh, K.C. Das, N. Tripathy, G. Bose, D.H. Kim, T. Lee, J.M. Myoung, J.P. Kar, Ammonia sensing behavior of zinc oxide thin films and nanostructures, IUP J. Electr. Electron. Eng. 9 (2016) 78–84.
[33] M. Calatayud, A. Markovits, M. Menetrey, B. Mguig, C. Minot, Adsorption on perfect and reduced surfaces of metal oxides, Catal. Today 85 (2003) 125–143, https://doi.org/10.1016/S0920-5861(03)00381-X.
[34] N. Barsan, U. Weimar, Conduction model of metal oxide gas sensors, J. Electroceram. 7 (2001) 143–167, https://doi.org/10.1023/A:1014405811371.
[35] L. Filipovic, S. Selberherr, Performance and stress analysis of metal oxide films for CMOS-integrated gas sensors, Sensors 15 (2015) 7206–7227, https://doi.org/10.3390/s150407206.
[36] H. Nanto, T. Minami, S. Takata, Zinc-oxide thin-film ammonia gas sensors with high sensitivity and excellent selectivity, J. Appl. Phys. 60 (1986) 482–484, https://doi.org/10.1063/1.337435.
[37] R.K. Srivastava, P. Lal, R. Dwivedi, S.K. Srivastava, Sensing mechanism in tin oxide-based thick-film gas sensors, Sensor. Actuator. B Chem. 21 (1994) 213–218.
[38] V. Srivastava, K. Jain, Highly sensitive NH3 sensor using Pt catalyzed silica coating over WO3 thick films, Sensor. Actuator. B Chem. 133 (2008) 46–52, https://doi.org/10.1016/j.snb.2008.01.066.
[39] K. Zakrzewska, Mixed oxides as gas sensors, Thin Solid Films 391 (2001) 229–238.
[40] P.T. Moseley, Progress in the development of semiconducting metal oxide gas sensors : a review, Meas. Sci. Technol. 28 (2017) 1–15.
[41] T. Li, W. Zeng, Z. Wang, Quasi-one-dimensional metal-oxide-based heterostructural gas-sensing materials: a review, Sensor. Actuator. B Chem. 221 (2015) 1570–1585, https://doi.org/10.1016/J.SNB.2015.08.003.
[42] G. Williams, G.S. V Coles, S. Park, Gas sensing properties of nanocrystalline metal oxide powders produced by a laser evaporation technique, J. Mater. Chem. 8 (1998) 1657–1664.
[43] J.F. Mcaleer, P.T. Moseley, J.W. Norris, D.E. Williams, B.C. Tofield, Tin dioxide gas sensors, J. Chem. Soc. Faraday. Trans. 84 (1988) 441–457.
[44] Y. Zeng, Z. Lou, L. Wang, B. Zou, T. Zhang, W. Zheng, G. Zou, Enhanced ammonia sensing performances of Pd-sensitized flowerlike ZnO nanostructure, Sensor. Actuator. B Chem. 156 (2011) 395–400, https://doi.org/10.1016/j.snb.2011.04.064.
[45] V.R. Shinde, T.P. Gujar, C.D. Lokhande, Enhanced response of porous ZnO nanobeads towards LPG: effect of Pd sensitization, Sensor. Actuator. B Chem. 123 (2007) 701–706, https://doi.org/10.1016/j.snb.2006.10.003.
[46] P.G. Su, L.Y. Yang, NH3gas sensor based on Pd/SnO2/RGO ternary composite operated at room-temperature, Sensor. Actuator. B Chem. 223 (2016) 202–208, https://doi.org/10.1016/j.snb.2015.09.091.
[47] Q. Qi, P.P. Wang, J. Zhao, L.L. Feng, L.J. Zhou, R.F. Xuan, Y.P. Liu, G.D. Li, SnO2 nanoparticle-coated In2O3 nanofibers with improved NH3 sensing properties, Sensor. Actuator. B Chem. 194 (2014) 440–446, https://doi.org/10.1016/j.snb.2013.12.115.
[48] X.J. Huang, Y.K. Choi, Chemical sensors based on nanostructured materials, Sensor. Actuator. B Chem. 122 (2007) 659–671, https://doi.org/10.1016/j.snb.2006.06.022.
[49] P. Bhattacharyya, P.K. Basu, H. Saha, S. Basu, Fast response methane sensor using nanocrystalline zinc oxide thin films derived by sol-gel method, Sensor. Actuator. B Chem. 124 (2007) 62–67, https://doi.org/10.1016/j.snb.2006.11.046.
[50] L. Francioso, M. Russo, A.M. Taurino, P. Siciliano, Micrometric patterning process of sol-gel SnO2, In2O3 and WO3 thin film for gas sensing applications: towards silicon technology integration, Sensor. Actuator. B Chem. 119 (2006) 159–166, https://doi.org/10.1016/j.snb.2005.12.006.
[51] L. Wang, Z. Lou, R. Zhang, T. Zhou, J. Deng, T. Zhang, Hybrid Co3O4/SnO2 core-shell nanospheres as real-time rapid-response sensors for ammonia gas, ACS Appl. Mater. Interfaces 8 (2016) 6539–6545, https://doi.org/10.1021/acsami.6b00305.
[52] J.J. Miasik, A. Hooper, B.C. Tofield, Conducting polymer gas sensors, J. Chem. Soc. Faraday Trans. 1 Phys. Chem. Condens. Phases. 82 (1986) 1117–1126.
[53] J. Janata, M. Josowicz, Conducting polymers in electronic chemical sensors, Nat. Mater. 2 (2002) 19–24.
[54] R. Balint, N.J. Cassidy, S.H. Cartmell, Conductive polymers: towards a smart biomaterial for tissue engineering, Acta Biomater. 10 (2014) 2341–2353, https://doi.org/10.1016/j.actbio.2014.02.015.
[55] Y. Wang, W. Jia, T. Strout, Y. Ding, Y. Lei, Preparation, characterization and sensitive gas sensing of conductive core-sheath TiO2-PEDOT nanocables, Sensors 9 (2009) 6752–6763, https://doi.org/10.3390/s90906752.
[56] R.S. Andre, J. Chen, D. Kwak, D.S. Correa, L.H.C. Mattoso, Y. Lei, A flexible and disposable poly(sodium 4-styrenesulfonate)/polyaniline coated glass microfiber paper for sensitive and selective detection of ammonia at room temperature, Synth. Met. 233 (2017) 22–27, https://doi.org/10.1016/j.synthmet.2017.08.005.
[57] R.S. Andre, D. Kwak, Q. Dong, W. Zhong, D.S. Correa, L.H.C. Mattoso, Y. Lei, Sensitive and selective NH3 monitoring at room temperature using ZnO ceramic nanofibers decorated with poly(Styrene sulfonate), Sensors 18 (2018) 1–13, https://doi.org/10.1080/01431160310001618725.
[58] Y. Wang, W. Jia, T. Strout, A. Schempf, H. Zhang, B. Li, J. Cui, Y. Lei, Ammonia gas sensor using polypyrrole-coated TiO2/ZnO nanofibers, Electroanalysis 21 (2009) 1432–1438, https://doi.org/10.1002/elan.200904584.
[59] A. Kassim, Z.B. Basar, H.N.M.E. Mahmud, Effects of preparation temperature on the conductivity of polypyrrole conducting polymer, Proc. Indian Acad. Sci. Chem. Sci. 114 (2002) 155–162, https://doi.org/10.1007/BF02704308.
[60] S. Virji, J. Huang, R.B. Kaner, B.H. Weiller, Polyaniline nanofiber gas sensors: examination of response mechanisms, Nano Lett. 4 (2004) 491–496, https://doi.org/10.1021/nl035122e.
[61] B.J. Privett, J.H. Shin, M.H. Schoenfisch, Electrochemical Sensors, Anal. Chem. 82 (2010) 4723–4741, https://doi.org/10.1021/ac060637m.Electrochemical.
[62] J. Gebicki, B. Chachulski, Influence of analyte flow rate on signal and response time of the amperometric gas sensor with Nafion membrane, Electroanalysis 21 (2009) 1568–1576, https://doi.org/10.1002/elan.200804567.
[63] H. Bai, G. Shi, Gas sensors based on conducting polymers, Sensors 7 (2007) 267–307, https://doi.org/10.3390/s7030267.
[64] S. Carquigny, J.B. Sanchez, F. Berger, B. Lakard, F. Lallemand, Ammonia gas sensor based on electrosynthesized polypyrrole films, Talanta 78 (2009) 199–206, https://doi.org/10.1016/j.talanta.2008.10.056.
[65] T. Zhang, M.B. Nix, B.Y. Yoo, M.A. Deshusses, N.V. Myung, Electrochemically functionalized single-walled carbon nanotube gas sensor, Electroanalysis 18 (2006) 1153–1158, https://doi.org/10.1002/elan.200603527.
[66] H. Liu, J. Kameoka, D.A. Czaplewski, H.G. Craighead, Polymeric nanowire chemical sensor, Nano Lett. 4 (2004) 671–675, https://doi.org/10.1021/nl049826f.
[67] E. Kriván, C. Visy, R. Dobay, G. Harsányi, O. Berkesi, Irregular response of the polypyrrole films to H2S, Electroanalysis 12 (2000) 1195–1200.
[68] H. Yoon, Current trends in sensors based on conducting polymer nanomaterials, Nanomaterials 3 (2013) 524–549, https://doi.org/10.3390/nano3030524.
[69] A.L. Kukla, Y.M. Shirshov, S.A. Piletsky, Ammonia sensors based on sensitive polyaniline films, Sensor. Actuator. B Chem. 37 (1996) 135–140, https://doi.org/10.1016/S0925-4005(97)80128-1.
[70] Z. Du, C. Li, L. Li, H. Yu, Y. Wang, T. Wang, Ammonia gas detection based on polyaniline nanofibers coated on interdigitated array electrodes, J. Mater. Sci. Mater. Electron. 22 (2011) 418–421, https://doi.org/10.1007/s10854-010-0152-5.
[71] J.L. Wojkiewicz, V.N. Bliznyuk, S. Carquigny, N. Elkamchi, N. Redon, T. Lasri, A.A. Pud, S. Reynaud, Nanostructured polyaniline-based composites for ppb range ammonia sensing, Sensor. Actuator. B Chem. 160 (2011) 1394–1403, https://doi.org/10.1016/j.snb.2011.09.084.
[72] G. Rizzo, A. Arena, N. Donato, M. Latino, G. Saitta, A. Bonavita, G. Neri, Flexible, all-organic ammonia sensor based on dodecylbenzene sulfonic acid-doped polyaniline films, Thin Solid Films 518 (2010) 7133–7137, https://doi.org/10.1016/j.tsf.2010.07.016.
[73] A. Choudhury, Polyaniline/silver nanocomposites: dielectric properties and ethanol vapour sensitivity, Sensor. Actuator. B Chem. 138 (2009) 318–325, https://doi.org/10.1016/j.snb.2009.01.019.
[74] A.A. Athawale, S.V. Bhagwat, Synthesis and characterization of novel copper/polyaniline nanocomposite and application as a catalyst in the Wacker oxidation reaction, J. Appl. Polym. Sci. 89 (2003) 2412–2417, https://doi.org/10.1002/app.12377.
[75] C. Van Tuan, M.A. Tuan, N. Van Hieu, T. Trung, Electrochemical synthesis of polyaniline nanowires on Pt interdigitated microelectrode for room temperature NH3 gas sensor application, Curr. Appl. Phys. 12 (2012) 1011–1016, https://doi.org/10.1016/j.cap.2011.12.006.
[76] U.V. Patil, N.S. Ramgir, N. Karmakar, A. Bhogale, A.K. Debnath, D.K. Aswal, S.K. Gupta, D.C. Kothari, Room temperature ammonia sensor based on copper nanoparticle intercalated polyaniline nanocomposite thin films, Appl. Surf. Sci. 339 (2015) 69–74, https://doi.org/10.1016/j.apsusc.2015.02.164.
[77] R. Peeters, G. Berden, A. Apituley, G. Meijer, Open-path trace gas detection of ammonia based on cavity-enhanced absorption spectroscopy, Appl. Phys. B 71 (2000) 231–236, https://doi.org/10.1007/s003400000302.
[78] X. Liu, S. Cheng, H. Liu, S. Hu, D. Zhang, H. Ning, A survey on gas sensing technology, Sensors 12 (2012) 9635–9665, https://doi.org/10.3390/s120709635.
[79] R. Kincaid, K. Johnson, G.H. Mount, D. Yonge, J. Havig, H. Westberg, B. Lamb, B. Rumburg, Measurement of atmospheric ammonia at a dairy using differential optical absorption spectroscopy in the mid-ultraviolet, Atmos. Environ. 36 (2002) 1799–1810, https://doi.org/10.1016/S1352-2310(02)00158-9.
[80] J. Hodgkinson, R.P. Tatam, Optical gas sensing: a review, Meas. Sci. Technol. 24 (2013), https://doi.org/10.1088/0957-0233/24/1/012004.
[81] J.S. Warland, G.M. Dias, G.W. Thurtell, A tunable diode laser system for ammonia flux measurements over multiple plots, Environ. Pollut. 114 (2001) 215–221, https://doi.org/10.1016/S0269-7491(00)00218-9.
[82] R. Claps, F. V Englich, D.P. Leleux, D. Richter, F.K. Tittel, R.F. Curl, Ammonia detection by use of near-infrared diode-laser-based overtone spectroscopy, Appl. Opt. 40 (2001) 4387–4394, https://doi.org/10.1364/AO.40.004387.
[83] M.E. Webber, D.S. Baer, R.K. Hanson, Ammonia monitoring near 15 μm with diode-laser absorption sensors, Appl. Opt. 40 (2001) 2031–2042, https://doi.org/10.1364/AO.40.002031.
[84] P.W. Werle, Diode-laser sensors for in-situ gas analysis, Laser Environ. Life Sci. 2004, pp. 223–243, , https://doi.org/10.1007/978-3-662-08255-3_11.

[85] P. Werle, F. Slemr, K. Maurer, R. Kormann, R. Mücke, B. Jänker, Near- and mid-incrared laser-optical sensors for gas analysis, Optic Laser. Eng. 37 (2002) 101–114, https://doi.org/10.1016/S0143-8166(01)00092-6.
[86] P. Werle, Tunable diode laser absorption spectroscopy: recent findings and novel approaches, Infrared Phys. Technol. 37 (1996) 59–66, https://doi.org/10.1016/1350-4495(95)00113-1.
[87] J. Li, B. Yu, W. Zhao, W. Chen, A review of signal enhancement and noise reduction techniques for tunable diode laser absorption spectroscopy, Appl. Spectrosc. Rev. 49 (2014) 666–691, https://doi.org/10.1080/05704928.2014.903376.
[88] H. Nasim, Y. Jamil, Recent advancements in spectroscopy using tunable diode lasers, Laser Phys. Lett. 10 (2013), https://doi.org/10.1088/1612-2011/10/4/043001.
[89] B. Panella, D. Maas, H. Brändle, B. Galletti, Highly sensitive tunable diode laser absorption spectroscopy for process and emission monitoring, Renew. Energy Environ. OSA Tech. Dig. (Optical Soc. Am. OSA publishing, Tucson, Arizona, United States, 2013EW1A.3 https://doi.org/10.1364/E2.2013.EW1A.3.
[90] F.K. Tittel, R. Lewicki, Tunable mid-infrared laser absorption spectroscopy, Semicond. Lasers, 2013, pp. 579–630, , https://doi.org/10.1533/9780857096401.3.579.
[91] S. Michael, W.W. Chow, H.C. Schneider, Mid-infrared quantum-dot quantum cascade Laser : a theoretical feasibility study, Photonics 3 (2016) 1–12, https://doi.org/10.3390/photonics3020029.
[92] A. Kosterev, G. Wysocki, Y. Bakhirkin, S. So, R. Lewicki, M. Fraser, F. Tittel, R.F. Curl, Application of quantum cascade lasers to trace gas analysis, Appl. Phys. B Laser Opt. 90 (2008) 165–176, https://doi.org/10.1007/s00340-007-2846-9.
[93] R. Maulini, D.A. Yarekha, J.-M. Bulliard, M. Giovannini, J. Faist, E. Gini, Continuous-wave operation of a broadly tunable thermoelectrically cooled external cavity quantum-cascade laser, Opt. Lett. 30 (2005) 2584–2586, https://doi.org/10.1364/OL.30.002584.
[94] G. Wysocki, R.F. Curl, F.K. Tittel, R. Maulini, J.M. Bulliard, J. Faist, Widely tunable mode-hop free external cavity quantum cascade laser for high resolution spectroscopic applications, Appl. Phys. B Laser Opt. 81 (2005) 769–777, https://doi.org/10.1007/s00340-005-1965-4.
[95] T. Aellen, S. Blaser, M. Beck, D. Hofstetter, J. Faist, E. Gini, Continuous-wave distributed-feedback quantum-cascade lasers on a Peltier cooler, Appl. Phys. Lett. 83 (2003) 1929–1931, https://doi.org/10.1063/1.1609044.
[96] B. Meng, Q.J. Wang, Broadly tunable single-mode mid-infrared quantum cascade lasers, J. Opt. 17 (2015) 1–20, https://doi.org/10.1088/2040-8978/17/2/023001.
[97] T. Liu, K.E. Lee, Q.J. Wang, Importance of the microscopic effects on the linewidth enhancement factor of quantum cascade lasers, Optic Express 21 (2013) 27804–27815, https://doi.org/10.1364/OE.21.027804.
[98] R.F. Curl, F. Capasso, C. Gmachl, A.A. Kosterev, B. McManus, R. Lewicki, M. Pusharsky, G. Wysocki, F.K. Tittel, Quantum cascade lasers in chemical physics, Chem. Phys. Lett. 487 (2010) 1–18, https://doi.org/10.1016/j.cplett.2009.12.073.
[99] N. Mukherjee, R. Go, C.K.N. Patel, Linewidth measurement of external grating cavity quantum cascade laser using saturation spectroscopy, Appl. Phys. Lett. 92 (2008) 1–4, https://doi.org/10.1063/1.2901038.
[100] N. Mukherjee, C.K.N. Patel, Molecular fine structure and transition dipole moment of NO2 using an external cavity quantum cascade laser, Chem. Phys. Lett. 462 (2008) 10–13, https://doi.org/10.1016/j.cplett.2008.07.050.
[101] T. Laurila, H. Cattaneo, V. Koskinen, J. Kauppinen, R. Hernberg, Diode laser-based photoacoustic spectroscopy with interferometrically-enhanced cantilever detection, Optic Express 13 (2005) 2453–2458, https://doi.org/10.1364/OPEX.13.002453.
[102] S.G. Baran, G. Hancock, R. Peverall, G.A.D. Ritchie, N.J. van Leeuwen, Optical feedback cavity enhanced absorption spectroscopy with diode lasers, Analyst 134 (2009) 243–249, https://doi.org/10.1039/B811793D.
[103] K. Namjou, S. Cai, E.A. Whittaker, J. Faist, C. Gmachl, F. Capasso, D.L. Sivco, A.Y. Cho, Sensitive absorption spectroscopy with a room-temperature distributed-feedback quantum-cascade laser, Opt. Lett. 23 (1998) 219–221, https://doi.org/10.1364/OL.23.000219.
[104] D.J. Miller, K. Sun, L. Tao, M.A. Khan, M.A. Zondlo, Open-path, quantum cascade-laser-based sensor for high-resolution atmospheric ammonia measurements, Atmos. Meas. Tech. 7 (2014) 81–93, https://doi.org/10.5194/amt-7-81-2014.
[105] P. Werle, R. Mücke, F. Slemr, The limits of signal averaging in atmospheric trace-gas monitoring by tunable diode-laser absorption spectroscopy (TDLAS), Appl. Phys. B Photophysics Laser Chem. 57 (1993) 131–139, https://doi.org/10.1007/BF00425997.
[106] L. Tao, K. Sun, D.J. Miller, D. Pan, L.M. Golston, M.A. Zondlo, Low-power, open-path mobile sensing platform for high-resolution measurements of greenhouse gases and air pollutants, Appl. Phys. B Laser Opt. 119 (2015) 153–164, https://doi.org/10.1007/s00340-015-6069-1.
[107] R. Lewicki, A.A. Kosterev, D.M. Thomazy, T.H. Risby, S. Solga, T.B. Schwartz, F.K. Tittel, Real time ammonia detection in exhaled human breath using a distributed feedback quantum cascade laser based sensor, Quantum Sens. Nanophotonic Devices VIII, Society of Photo-Optical Instrumentation Engineers (SPIE), San Francisco, California, USA, 2011, pp. 79450K1–79450K7, https://doi.org/10.1117/12.874887.
[108] M.J. Malachowski, J. Zmija, Ultrasensitive laser spectroscopy for breath analysis, Opto-Electron. Rev. 18 (2010) 121–136, https://doi.org/10.2478/s11772.
[109] D.B. Atkinson, Solving chemical problems of environmental importance using cavity ring-down spectroscopy, Analyst 128 (2003) 117–125, https://doi.org/10.1039/b206699h.
[110] Y. He, C. Jin, R. Kan, J. Liu, W. Liu, J. Hill, I.M. Jamie, B.J. Orr, Remote open-path cavity-ringdown spectroscopic sensing of trace gases in air, based on distributed passive sensors linked by km-long optical fibers, Optic Express 22 (2014) 13170–13189, https://doi.org/10.1364/OE.22.013170.
[111] L. Xiong, R.G. Compton, Amperometric gas detection: a review, Int. J. Electrochem. Sci. 9 (2014) 7152–7181.
[112] J. Wang, Analytical Electrochemistry, John Wiley & Sons, Inc., Hoboken, NJ, USA, 2006, https://doi.org/10.1002/0471790303.
[113] E.I. Rogers, A.M.O. Mahony, L. Aldous, R.G. Compton, Amperometric gas detection using room temperature ionic liquid solvents, ECS Trans 33 (2010) 473–502.
[114] X. Ji, C.E. Banks, R.G. Compton, The electrochemical oxidation of ammonia at boron-doped diamond electrodes exhibits analytically useful signals in aqueous solutions, Analyst 130 (2005) 1345–1347, https://doi.org/10.1039/b508975a.
[115] S.G. Sazhin, E.I. Soborover, S.V. Tokarev, Sensor methods of ammonia inspection, Russ. J. Nondestr. Test. 39 (2003) 791–806, https://doi.org/10.1023/B:RUNT.0000020251.56686.a5.
[116] B.H. King, A. Gramada, J.R. Link, M.J. Sailor, Internally referenced ammonia sensor based on an electrochemically prepared porous SiO2 photonic crystal, Adv. Mater. 19 (2007) 4044–4048, https://doi.org/10.1002/adma.200602860.
[117] M.E. Meyerhoff, Polymer membrane electrode based potentiometric ammonia gas sensor, Anal. Chem. 52 (1980) 1532–1534, https://doi.org/10.1021/ac50059a037.
[118] R. Toniolo, N. Dossi, A. Pizzariello, A.P. Doherty, G. Bontempelli, A membrane free amperometric gas sensor based on room temperature ionic liquids for the selective monitoring of NOx, Electroanalysis 24 (2012) 865–871, https://doi.org/10.1002/elan.201100496.
[119] N. Dossi, R. Toniolo, A. Pizzariello, E. Carrilho, E. Piccin, S. Battiston, G. Bontempelli, An electrochemical gas sensor based on paper supported room temperature ionic liquids, Lab Chip 12 (2012) 153–158, https://doi.org/10.1039/c1lc20663j.
[120] R. Toniolo, N. Dossi, A. Pizzariello, A. Casagrande, G. Bontempelli, Electrochemical gas sensors based on paper-supported room-temperature ionic liquids for improved analysis of acid vapours, Anal. Bioanal. Chem. 405 (2013) 3571–3577, https://doi.org/10.1007/s00216-012-6588-0.
[121] L. Xiong, P. Goodrich, C. Hardacre, R.G. Compton, Evaluation of a simple disposable microband electrode device for amperometric gas sensing, Sensor. Actuator. B Chem. 188 (2013) 978–987, https://doi.org/10.1016/j.snb.2013.07.104.
[122] X.J. Huang, L. Aldous, A.M. Omahony, F.J. Del Campo, R.G. Compton, Toward membrane-free amperometric gas sensors: a microelectrode array approach, Anal. Chem. 82 (2010) 5238–5245, https://doi.org/10.1021/ac1006359.
[123] J. Lee, G. Du Plessis, D.W.M. Arrigan, D.S. Silvester, Towards improving the robustness of electrochemical gas sensors: impact of PMMA addition on the sensing of oxygen in an ionic liquid, Anal. Methods. 7 (2015) 7327–7335, https://doi.org/10.1039/c5ay00497g.
[124] M.C. Buzzeo, C. Hardacre, R.G. Compton, Use of room temperature ionic liquids in gas sensor design, Anal. Chem. 76 (2004) 4583–4588, https://doi.org/10.1021/ac040042w.
[125] R. Toniolo, A. Pizzariello, S. Susmel, N. Dossi, A.P. Doherty, G. Bontempelli, An ionic-liquid based probe for the sequential preconcentration from headspace and direct voltammetric detection of phenols in wastewaters, Electroanalysis 19 (2007) 2141–2148, https://doi.org/10.1002/elan.200703961.
[126] J. Gębicki, A. Kloskowski, W. Chrzanowski, P. Stepnowski, J. Namiesnik, Application of ionic liquids in amperometric gas sensors, Crit. Rev. Anal. Chem. 46 (2016) 122–138, https://doi.org/10.1080/10408347.2014.989957.
[127] X. Mu, S. Member, Z. Wang, X. Zeng, A.J. Mason, S. Member, A robust flexible electrochemical gas sensor using room temperature ionic liquid, IEEE Sens. J. 13 (2013) 3976–3981.
[128] L.E. Barrosse-Antle, A.M. Bond, R.G. Compton, A.M. O'Mahony, E.I. Rogers, D.S. Silvester, Voltammetry in room temperature ionic liquids: comparisons and contrasts with conventional electrochemical solvents, Chem. Asian J. 5 (2010) 202–230, https://doi.org/10.1002/asia.200900191.
[129] X. Ji, D.S. Silvester, L. Aldous, C. Hardacre, R.G. Compton, Mechanistic studies of the electro-oxidation pathway of ammonia in several room-temperature ionic liquids, J. Phys. Chem. C 111 (2007) 9562–9572, https://doi.org/10.1021/jp0715732.
[130] R. Toniolo, R. Bortolomeazzi, R. Svigelj, N. Dossi, I.G. Casella, C. Bragato, S. Daniele, Use of an electrochemical room temperature ionic liquid-based microprobe for measurements in gaseous atmospheres, Sensor. Actuator. B Chem. 240 (2017) 239–247, https://doi.org/10.1016/j.snb.2016.08.139.
[131] J.F.M. Oudenhoven, W. Knoben, R. Van Schaijk, Electrochemical detection of ammonia using a thin ionic liquid film as the electrolyte, Procedia Eng 120 (2015) 983–986, https://doi.org/10.1016/j.proeng.2015.08.636.
[132] P.K. Sekhar, J.S. Kysar, An electrochemical ammonia sensor on paper substrate, J. Electrochem. Soc. 164 (2017) B113–B117, https://doi.org/10.1149/2.0941704jes.
[133] J. Sarfraz, P. Ihalainen, A. Määttänen, J. Peltonen, M. Lindén, Printed hydrogen sulfide gas sensor on paper substrate based on polyaniline composite, Thin Solid Films 534 (2013) 621–628, https://doi.org/10.1016/j.tsf.2013.02.055.
[134] S.K. Mahadeva, K. Walus, B. Stoeber, Paper as a platform for sensing applications and other devices: a review, ACS Appl. Mater. Interfaces 7 (2015) 8345–8362, https://doi.org/10.1021/acsami.5b00373.
[135] J. Zhang, L. Huang, Y. Lin, L. Chen, Z. Zeng, L. Shen, Q. Chen, W. Shi, Pencil-trace on printed silver interdigitated electrodes for paper-based NO2 gas sensors, Appl. Phys. Lett. 106 (2015) 1–5, https://doi.org/10.1063/1.4917063.
[136] W. Liu, Y. Liu, J. Do, J. Li, Highly sensitive room temperature ammonia gas sensor

based on Ir-doped Pt porous ceramic electrodes, Appl. Surf. Sci. 390 (2016) 929–935, https://doi.org/10.1016/j.apsusc.2016.08.121.
[137] E. Moran, C. Cattaneo, H. Mishima, B.A. López De Mishima, S.P. Silvetti, J.L. Rodriguez, E. Pastor, Ammonia oxidation on electrodeposited Pt-Ir alloys, J. Solid State Electrochem. 12 (2008) 583–589, https://doi.org/10.1007/s10008-007-0407-0.
[138] B.K. Boggs, G.G. Botte, Optimization of Pt-Ir on carbon fiber paper for the electro-oxidation of ammonia in alkaline media, Electrochim. Acta 55 (2010) 5287–5293, https://doi.org/10.1016/j.electacta.2010.04.040.
[139] S. Le Vot, L. Roué, D. Bélanger, Synthesis of Pt-Ir catalysts by coelectrodeposition: application to ammonia electrooxidation in alkaline media, J. Power Sources 223 (2013) 221–231, https://doi.org/10.1016/j.jpowsour.2012.08.048.
[140] K. Endo, Y. Katayama, T. Miura, Pt-Ir and Pt-Cu binary alloys as the electrocatalyst for ammonia oxidation, Electrochim. Acta 49 (2004) 1635–1638, https://doi.org/10.1016/S0013-4686(03)00993-9.
[141] T.H. Lin, Y.T. Li, H.C. Hao, I.C. Fang, C.M. Yang, D.J. Yao, Surface acoustic wave gas sensors for monitoring low concentration ammonia, 2011 16th Int. Solid-State Sensors, Actuators Microsystems Conf., IEEE, Beijing, China, 2011, pp. 1140–1143.
[142] J. Hlavay, G.G. Guilbault, Detection of ammonia in ambient air with coated piezoelectric crystal detector, Anal. Chem. 50 (1978) 1044–1046 http://www.scopus.com/scopus/inward/record.url?eid=2-s2.0-0018193869&partnerID=40&rel=R8.2.0.
[143] F. Winquist, A. Spetz, M. Armgarth, C. Nylander, I. Lundström, Modified palladium metal-oxide-semiconductor structures with increased ammonia gas sensitivity, Appl. Phys. Lett. 43 (1983) 839–841, https://doi.org/10.1063/1.94514.
[144] M. Penza, E. Milella, V.I. Anisimkin, Gas sensing properties of Langmuir-blodgett polypyrrole film investigated by surface acoustic waves, IEEE Trans. Ultrason. Ferroelectr. Freq. Control 45 (1998) 1125–1132.
[145] V.B. Raj, A.T. Nimal, Y. Parmar, M.U. Sharma, K. Sreenivas, V. Gupta, Cross-sensitivity and selectivity studies on ZnO surface acoustic wave ammonia sensor, Sensor. Actuator. B Chem. 147 (2010) 517–524, https://doi.org/10.1016/j.snb.2010.03.079.
[146] Y.-L. Tang, Z.-J. Li, J.-Y. Ma, Y.-J. Guo, Y.-Q. Fu, X.-T. Zu, Ammonia gas sensors based on ZnO/SiO2 bi-layer nanofilms on ST-cut quartz surface acoustic wave devices, Sensor. Actuator. B Chem. 201 (2014) 114–121, https://doi.org/10.1016/j.snb.2014.04.046.
[147] C.Y. Shen, C.P. Huang, W.T. Huang, Gas-detecting properties of surface acoustic wave ammonia sensors, Sensor. Actuator. B Chem. 101 (2004) 1–7, https://doi.org/10.1016/j.snb.2003.07.016.
[148] B. Drafts, Acoustic wave technology sensors, IEEE Trans. Microw. Theory Tech. 49 (2001) 795–802, https://doi.org/10.1109/22.915466.
[149] X. Chen, D.M. Li, S.F. Liang, S. Zhan, M. Liu, Gas sensing properties of surface acoustic wave NH3 gas sensor based on Pt doped polypyrrole sensitive film, Sensor. Actuator. B Chem. 177 (2013) 364–369, https://doi.org/10.1016/j.snb.2012.10.120.
[150] V.B. Raj, H. Singh, A.T. Nimal, M.U. Sharma, V. Gupta, Oxide thin films (ZnO, TeO2, SnO2, and TiO2) based surface acoustic wave (SAW) E-nose for the detection of chemical warfare agents, Sensor. Actuator. B Chem. 178 (2013) 636–647, https://doi.org/10.1016/j.snb.2012.12.074.
[151] D. Xu, M. Guan, Q. Xu, Y. Guo, Multilayer films of layered double hydroxide/polyaniline and their ammonia sensing behavior, J. Hazard Mater. 262 (2013) 64–70, https://doi.org/10.1016/j.jhazmat.2013.08.034.
[152] Y. Wang, X. Wu, Q. Su, Y. Li, Z. Zhou, Ammonia-sensing characteristics of Pt and SiO2 doped SnO2 materials, Solid State Electron. 45 (2001) 347–350 http://www.sciencedirect.com/science/article/pii/S0038110100002318.
[153] G. Eranna, B.C. Joshi, D.P. Runthala, R.P. Gupta, Oxide materials for development of integrated gas sensors - a comprehensive review, Crit. Rev. Solid State Mater. Sci. 29 (2004) 111–188, https://doi.org/10.1080/10408430490888977.
[154] L. Wang, B. Han, L. Dai, Y. Li, H. Zhou, H. Wang, An amperometric NO2 sensor based on La10Si5NbO27.5 electrolyte nano-structured CuO sensing electrode, Mater. Lett. 109 (2013) 16–19, https://doi.org/10.1016/j.matlet.2013.07.032.
[155] S. Ma, R. Li, C. Lv, W. Xu, X. Gou, Facile synthesis of ZnO nanorod arrays and hierarchical nanostructures for photocatalysis and gas sensor applications, J. Hazard Mater. 192 (2011) 730–740, https://doi.org/10.1016/j.jhazmat.2011.05.082.
[156] S.Y. Wang, J.Y. Ma, Z.J. Li, H.Q. Su, N.R. Alkurd, W.L. Zhou, L. Wang, B. Du, Y.L. Tang, D.Y. Ao, S.C. Zhang, Q.K. Yu, X.T. Zu, Surface acoustic wave ammonia sensor based on ZnO/SiO2 composite film, J. Hazard Mater. 285 (2015) 368–374, https://doi.org/10.1016/j.jhazmat.2014.12.014.
[157] Y.L. Tang, Z.J. Li, J.Y. Ma, H.Q. Su, Y.J. Guo, L. Wang, B. Du, J.J. Chen, W. Zhou, Q.K. Yu, X.T. Zu, Highly sensitive room-temperature surface acoustic wave (SAW) ammonia sensors based on Co3O4/SiO2composite films, J. Hazard Mater. 280 (2014) 127–133, https://doi.org/10.1016/j.jhazmat.2014.08.001.
[158] P.T. Moseley, Solid state gas sensors, Meas. Sci. Technol. 8 (1997) 223–237 isi:A1997WM29900003.
[159] T.Y. Chen, H.I. Chen, C.S. Hsu, C.C. Huang, C.F. Chang, P.C. Chou, W.C. Liu, On an ammonia gas sensor based on a Pt/AlGaN heterostructure field-effect transistor, IEEE Electron. Device Lett. 33 (2012) 612–614, https://doi.org/10.1109/LED.2012.2184832.
[160] H. Wingbrant, Studies of MISiC-FET Sensors for Car Exhaust Gas Monitoring, Linköping University, 2005, http://liu.diva-portal.org/smash/record.jsf?pid=diva2:20684.
[161] H. Wingbrant, H. Svenningstorp, P. Salomonsson, D. Kubinski, J.H. Visser, M. Löfdahl, A.L. Spetz, Using a MISiC-FET sensor for detecting NH3 in SCR systems, IEEE Sens. J. 5 (2005) 1099–1105, https://doi.org/10.1109/JSEN.2005.854489.
[162] B. Ostrick, R. Pohle, M. Fleischer, H. Meixner, TiN in work function type sensors: a stable ammonia sensitive material for room temperature operation with low humidity cross sensitivity, Sensor. Actuator. B Chem. 68 (2000) 234–239, https://doi.org/10.1016/S0925-4005(00)00434-2.
[163] W. Huang, K. Besar, R. LeCover, A.M. Rule, P.N. Breysse, H.E. Katz, Highly sensitive NH3 detection based on organic field effect transistors with tris(pentafluorophenyl)borane as receptor, J. Am. Chem. Soc. 134 (2012) 14650–14653, https://doi.org/10.1016/j.immuni.2010.12.017.Two-stage.
[164] A. Klug, M. Denk, T. Bauer, M. Sandholzer, U. Scherf, C. Slugovc, E.J.W. List, Organic field-effect transistor based sensors with sensitive gate dielectrics used for low- concentration ammonia detection, Org. Electron. 14 (2013) 500–504 https://doi.org/10.1016/j.orgel.2012.11.030.
[165] J. Yu, X. Yu, L. Zhang, H. Zeng, Ammonia gas sensor based on pentacene organic field-effect transistor, Sensor. Actuator. B Chem. 173 (2012) 133–138, https://doi.org/10.1016/j.snb.2012.06.060.
[166] G.-S. Ryu, K.-H. Park, W.-T. Park, Y.-H. Kim, Y.-Y. Noh, High-performance diketopyrrolopyrrole-based organic field-effect transistors for flexible gas sensors, Org. Electron. 23 (2015) 76–81, https://doi.org/10.1016/j.orgel.2015.04.001.
[167] L. Li, P. Gao, M. Baumgarten, K. Müllen, N. Lu, H. Fuchs, L. Chi, High performance field-effect ammonia sensors based on a structured ultrathin organic semiconductor film, Adv. Mater. 25 (2013) 3419–3425, https://doi.org/10.1002/adma.201301138.
[168] R.F. Pierret, Semiconductor Device Fundamentals, (1996), https://doi.org/10.1007/BF00198606.
[169] Y. Chen, G. Xie, T. Xie, Y. Liu, H. Du, Y. Su, Y. Jiang, Thin film transistors based on poly(3-hexylthiophene)/[6,6]-phenyl C61 butyric acid methyl ester hetero-junction for ammonia detection, Chem. Phys. Lett. 638 (2015) 87–93, https://doi.org/10.1016/j.cplett.2015.07.026.
[170] S. Han, X. Zhuang, W. Shi, X. Yang, L. Li, J. Yu, Poly(3-hexylthiophene)/polystyrene(P3HT/PS) blends based organic field-effect transistor ammonia gas sensor, Sensor. Actuator. B Chem. 225 (2016) 10–15 https://doi.org/10.1016/j.snb.2015.11.005.
[171] T. Xie, G. Xie, Y. Zhou, J. Huang, M. Wu, Y. Jiang, H. Tai, Thin film transistors gas sensors based on reduced graphene oxide poly(3-hexylthiophene) bilayer film for nitrogen dioxide detection, Chem. Phys. Lett. 614 (2015) 275–281 https://doi.org/10.1016/j.cplett.2014.09.028.
[172] K. Besar, S. Yang, X. Guo, W. Huang, A.M. Rule, P.N. Breysse, I.J. Kymissis, H.E. Katz, Printable ammonia sensor based on organic field effect transistor, Org. Electron. 15 (2014) 3221–3230, https://doi.org/10.1016/j.orgel.2014.08.023.
[173] C. Kumar, G. Rawat, H. Kumar, Y. Kumar, R. Prakash, S. Jit, Electrical and ammonia gas sensing properties of poly (3, 3‴- dialkylquaterthiophene) based organic thin film transistors fabricated by floating-film transfer method, Org. Electron. 48 (2017) 53–60, https://doi.org/10.1016/j.orgel.2017.05.040.
[174] J. Yu, X. Yu, L. Zhang, H. Zeng, Ammonia gas sensor based on pentacene organic field-effect transistor, Sensor. Actuator. B Chem. 173 (2012) 133–138, https://doi.org/10.1016/j.snb.2012.06.060.
[175] S. Han, X. Zhuang, Y. Jiang, X. Yang, L. Li, J. Yu, Poly(vinyl alcohol) as a gas accumulation layer for an organic field-effect transistor ammonia sensor, Sensor. Actuator. B Chem. 243 (2017) 1248–1254, https://doi.org/10.1016/j.snb.2016.12.116.
[176] M.Z. Dai, Y.H. Chen, M.Y. Chuang, H.W. Zan, H.F. Meng, Achieving a good life time in a vertical-organic-diode gas sensor, Sensors 14 (2014) 16287–16295, https://doi.org/10.3390/s140916287.
[177] S. Tiwari, A.K. Singh, L. Joshi, P. Chakrabarti, W. Takashima, K. Kaneto, R. Prakash, Poly-3-hexylthiophene based organic field-effect transistor : detection of low concentration of ammonia, Sensor. Actuator. B Chem. 171–172 (2012) 962–968, https://doi.org/10.1016/j.snb.2012.06.010.
[178] E.A. Baum, T.J. Lewis, R. Toomer, The lateral motion of charge on thin films of polyethylene terephthalate, J. Phys. D Appl. Phys. 11 (1978) 963–977, https://doi.org/10.1088/0022-3727/11/6/016.
[179] L. Herous, M. Remadnia, M. Kachi, M. Nemamcha, Decay of electrical charges on polyethylene Terephthalate surface, J. Eng. Sci. Technol. Rev. 2 (2009) 87–90, https://doi.org/10.25103/jestr.021.17.
[180] T. Mizutani, T. Oomura, M. Ieda, Surface Potential decay in polyethylene, Jpn. J. Appl. Phys. 20 (1981) 855–859.
[181] R.K. Pandey, W. Takashima, S. Nagamatsu, A. Dauendorffer, K. Kaneto, R. Prakash, Macroscopic self ordering of solution processible poly(3,3‴- dialkylquaterthiophene) by floating film transfer method, J. Appl. Phys. 114 (2013) 1–5, https://doi.org/10.1063/1.4817288.
[182] I. Kang, H. Yun, D.S. Chung, S. Kwon, Y. Kim, Record high hole mobility in polymer semiconductors via side-chain engineering, J. Am. Chem. Soc. 135 (2013) 14896–14899, https://doi.org/10.1021/ja405112s.
[183] W. Wang, S.K. Hwang, K.L. Kim, J.H. Lee, S.M. Cho, C. Park, Highly reliable top-gated thin-film transistor memory with semiconducting, tunneling, charge-trapping, and blocking layers all of flexible polymers, ACS Appl. Mater. Interfaces 7 (2015) 10957–10965, https://doi.org/10.1021/acsami.5b02213.
[184] S.H. Yu, J. Cho, K.M. Sim, J.U. Ha, D.S. Chung, Morphology-driven high-performance polymer transistor-based ammonia gas sensor, ACS Appl. Mater. Interfaces 8 (2016) 6570–6576, https://doi.org/10.1021/acsami.6b00471.
[185] K.H. Cheon, J. Cho, Y.H. Kim, D.S. Chung, Thin film transistor gas sensors incorporating high-mobility diketopyrrolopyrole-based polymeric semiconductor doped with graphene oxide, ACS Appl. Mater. Interfaces 7 (2015) 14004–14010, https://doi.org/10.1021/acsami.5b03059.
[186] L.G. Kaake, P.F. Barbara, X.Y. Zhu, Intrinsic charge trapping in organic and polymeric semiconductors: a physical chemistry perspective, J. Phys. Chem. Lett. 1

(2010) 628–635, https://doi.org/10.1021/jz9002857.
[187] G. Pfister, Hopping transport in a molecularly doped organic polymer, Phys. Rev. B 16 (1977) 3676–3687.
[188] J. Zhang, Z. Qin, D. Zeng, C. Xie, Metal-oxide-semiconductor based gas sensors: screening, preparation, and integration, Phys. Chem. Chem. Phys. 19 (2017) 6313–6329, https://doi.org/10.1039/c6cp07799d.
[189] N.T. Kemp, A.B. Kaiser, H.J. Trodahl, B. Chapman, R.G. Buckley, A.C. Partridge, P.J.S. Foot, Effect of ammonia on the temperature-dependent conductivity and thermopower of polypyrrole, J. Polym. Sci., Part B: Polym. Phys. 44 (2006) 1331–1338, https://doi.org/10.1002/polb.
[190] M.-Y. Kuo, H.-Y. Chen, I. Chao, Cyanation, Providing a three-in-one advantage for the design of n-type organic field-effect transistors, Chem. Eur J. 13 (2007) 4750–4758, https://doi.org/10.1002/chem.200601803.
[191] P. Dhivya, A.K. Prasad, M. Sridharan, Nanostructured TiO2films: Enhanced NH3detection at room temperature, Ceram. Int. 40 (2014) 409–415, https://doi.org/10.1016/j.ceramint.2013.06.016.
[192] S. Xu, K. Kan, Y. Yang, C. Jiang, J. Gao, L. Jing, P. Shen, L. Li, K. Shi, Enhanced NH3 gas sensing performance based on electrospun alkaline-earth metals composited SnO2 nanofibers, J. Alloys Compd. 618 (2015) 240–247, https://doi.org/10.1016/j.jallcom.2014.08.153.
[193] J. Wang, P. Yang, X. Wei, High-performance, room-temperature, and no-humidity-impact ammonia sensor based on heterogeneous nickel oxide and zinc oxide nanocrystals, ACS Appl. Mater. Interface. 7 (2015) 3816–3824, https://doi.org/10.1021/am508807a.
[194] G.H. Mhlongo, D.E. Motaung, H.C. Swart, Pd^{2+} doped ZnO nanostructures: Structural, luminescence and gas sensing properties, Mater. Lett. 160 (2015) 200–205, https://doi.org/10.1016/j.matlet.2015.07.139.
[195] C. Sun, P.K. Dutta, Selective detection of part per billion concentrations of ammonia using a p-n semiconducting oxide heterostructure, Sens. Actuat. B Chem. 226 (2016) 156–169, https://doi.org/10.1016/j.snb.2015.11.085.
[196] Y. Chen, W. Zhang, Q. Wu, A highly sensitive room-temperature sensing material for NH3:SnO2-nanorods coupled by rGO, Sens. Actuat. B Chem. 242 (2017) 1216–1226, https://doi.org/10.1016/j.snb.2012.02.076.
[197] Z. Ye, H. Tai, R. Guo, Z. Yuan, C. Liu, Y. Su, Z. Chen, Y. Jiang, Excellent ammonia sensing performance of gas sensor based on graphene/titanium dioxide hybrid with improved morphology, Appl. Surf. Sci. 419 (2017) 84–90, https://doi.org/10.1016/j.apsusc.2017.03.251.
[198] R. Sankar Ganesh, E. Durgadevi, M. Navaneethan, V.L. Patil, S. Ponnusamy, C. Muthamizhchelvan, S. Kawasaki, P.S. Patil, Y. Hayakawa, Low temperature ammonia gas sensor based on Mn-doped ZnO nanoparticle decorated microspheres, J. Alloy. Compd. 721 (2017) 182–190, https://doi.org/10.1016/j.jallcom.2017.05.315.
[199] A. Sharma, P. Bhojane, A.K. Rana, Y. Kumar, P.M. Shirage, Mesoporous nickel cobalt hydroxide/oxide as an excellent room temperature ammonia sensor, Scr. Mater 128 (2017) 65–68, https://doi.org/10.1016/j.scriptamat.2016.10.003.
[200] D. Zhang, C. Jiang, Y. Sun, Room-temperature high-performance ammonia gas sensor based on layer-by-layer self-assembled molybdenum disulfide/zinc oxide nanocomposite film, J. Alloy. Compd. 698 (2017) 476–483, https://doi.org/10.1016/j.jallcom.2016.12.222.
[201] Z. Wu, X. Chen, S. Zhu, Z. Zhou, Y. Yao, W. Quan, B. Liu, Enhanced sensitivity of ammonia sensor using graphene/polyaniline nanocomposite, Sens. Actuat. B Chem. 178 (2013) 485–493, https://doi.org/10.1016/j.snb.2013.01.014.
[202] S. Sharma, S. Hussain, S. Singh, S.S. Islam, MWCNT-conducting polymer composite based ammonia gas sensors : A new approach for complete recovery process, Sens. Actuat. B Chem. 194 (2014) 213–219, https://doi.org/10.1016/j.snb.2013.12.050.
[203] G. Zhu, Q. Zhang, G. Xie, Y. Su, K. Zhao, H. Du, Y. Jiang, Gas sensors based on polyaniline / zinc oxide hybrid film for ammonia detection at room temperature, Chem. Phys. Lett. 665 (2016) 147–152, https://doi.org/10.1016/j.cplett.2016.10.068.
[204] D.J. Miller, K. Sun, L. Tao, M.A. Khan, M.A. Zondlo, Open-path, quantum cascade-laser-based sensor for high-resolution atmospheric ammonia measurements, Atmos. Meas. Tech. (2014), https://doi.org/10.5194/amt-7-81-2014.